U.S.N.A. -- Trident Scholar project report; no. 275 (2000)

"The Effects of Thermal Shock on Pressure Transducers in Internal Combustion Engines"

by

Midshipman William M. Mathis, Class of 2000
United States Naval Academy
Annapolis, Maryland

Certification of Advisor Approval

Assistant Professor Paulius V Puzinauskas
Department of Mechanical Engineering

Acceptance for the Trident Scholar Committee

Professor Joyce E. Shade
Chair, Trident Scholar Committee

Report Date *("DD MON YYYY")* 08-05-2000	Report Type N/A	Dates Covered (from... to) *("DD MON YYYY")*

Title and Subtitle The Effects of Thermal Shock on Pressure Transducers in Internal Combustion Engines	**Contract or Grant Number**
	Program Element Number
Authors Mathis, William M.	**Project Number**
	Task Number
	Work Unit Number
Performing Organization Name(s) and Address(es) U.S. Naval Academy Annapolis, MD	**Performing Organization Number(s)**
Sponsoring/Monitoring Agency Name(s) and Address(es)	**Monitoring Agency Acronym**
	Monitoring Agency Report Number(s)
Distribution/Availability Statement Approved for public release, distribution unlimited	
Supplementary Notes Accepted by the U.S. Trident Scholar Committee	

Abstract
The objective of this project is to characterize engine-combustion-pressure measurement errors caused by flame induced transducer thermal stress. Thermal shock measured in an engine flame simulator was compared to data from a running engine. The engine-flame simulator impinged an oxygen-acetylene flame on a pressure transducer at atmospheric pressure. At constant pressure, any change in the transducers output can be attributed to thermal shock. This identifies the exact instant at which thermal shock begins and the start of its subsequent recovery.

Subject Terms
thermal shock; pressure transducers; internal combustion engine

Document Classification unclassified	**Classification of SF298** unclassified
Classification of Abstract unclassified	**Limitation of Abstract** unlimited
Number of Pages 62	

ABSTRACT

The objective of this project is to characterize engine-combustion-pressure measurement errors caused by flame induced transducer thermal stress. Thermal shock measured in an engine flame simulator was compared to data from a running engine. The engine-flame simulator impinged an oxygen-acetylene flame on a pressure transducer at atmospheric pressure. At constant pressure, any change in the transducer's output can be attributed to thermal shock. This identifies the exact instant at which thermal shock begins and the start of its subsequent recovery.

Engine measurements compared the full cycle output to a reference transducer, mounted lower in the cylinder. This transducer was not exposed to combustion chamber gases until after combustion was complete; hence it was effectively protected from thermal shock. Heat flux data were simultaneously measured. The tests were performed using a miniature transducer representative of the current state-of-the-art transducers and a large, water-cooled pressure transducer.

The recovery periods of both transducers contained both a linear component and an exponential component. The linear component appeared to be related to the thermal drift, while the exponential component appeared to correlate linearly with heat flux magnitude. In the engine, recovery from thermal shock continued throughout the engine cycle except at very low speed.

KEY WORDS

Thermal Shock, Pressure Transducers, Internal Combustion Engine

ACKNOWLEDGMENTS

I would like to thank Professor Puzinauskas for encouraging me to pursue excellence. I have learned many valuable lessons from him that I will be able to apply in graduate school and in life.

I would like to thank the Bob Woody and his technical support team for helping me out and I would also like to thank my parents for their awesome support.

Thank you.

TABLE OF CONTENTS

INTRODUCTION

OVERVIEW

The objective of this project was to characterize engine combustion-pressure-measurement errors caused by flame-induced transducer thermal stress. A cylinder-pressure transducer's surface temperature rises rapidly when the flame-front arrives. The associated thermal gradient causes a stress on the sensing element, thereby causing an error in the measurement. This report describes an experiment to quantify and characterize this error. Additional background will be provided which describes this error and how it may affect engine combustion system development. The following sections present the technical approach used, discussion of results, as well as conclusions and recommendations for further work.

BACKGROUND

It is widely accepted by the engine industry that cycle-resolved engine-cylinder pressure is one of the most important measurements for the quantification and improvement of engine combustion-system performance. All other properties exist with large spatial gradients and are nearly impossible to characterize with a single point measurement.

Currently, engine cylinder-pressure data are usually obtained with piezo-electric pressure transducers. These transducers have adequate frequency response, durability, and repeatability. Under steady thermal conditions their absolute accuracy can be

substantially better than one percent.[1] However, their accuracy is degraded when they are exposed to the transient flame resulting from the cylinder combustion process. A significant error occurs when the combustion flame blasts the position of the transducer. The rapid increase in temperature causes the transducer's diaphragm to momentarily deform in response to the thermal stress. The erroneous pressure data caused by this deformation is called thermal shock. To date, most of the efforts to reduce thermal shock have focused on designing and mounting the transducers to minimize the magnitude of these errors.[2] While these efforts have yielded improvements in accuracy, the problem remains.

Figure 1 shows an example of cycle-resolved combustion pressure plotted vs. crankshaft angle (1a) and volume (1b) measured in a spark-ignition internal combustion engine. The volume is calculated from the crankshaft angle and knowledge of the engine geometry. The relationship between pressure and crankshaft angle is typically fixed by triggering the pressure measurement with a crankshaft encoder. This encoder sends a signal to the data acquisition system to sample the pressure every time the crankshaft rotates through a fixed angle. This sample resolution typically varies from 0.1 degrees in diesel engines to 1.0 degrees in a spark-ignition engine. If the measurement is made fast enough to resolve how the pressure changes throughout the engine cycle it is termed cycle-resolved. A cycle-resolved plot can contain data from a single engine cycle or may be constructed by averaging over a few degrees of crank-angle for many consecutive cycles. Such an average is called an ensemble average.

There are many useful measurements and calculations that can be obtained from cylinder-pressure data and used in the development of engines, such as the following:

- The peak pressure and the maximum pressure gradient determine the material strength required to withstand the forces created by the combustion process.

- Net indicated mean effective pressure (NIMEP), which is the volume weighted average pressure, is proportional to the work per cycle. This work can be compared to work measured at the flywheel to determine mechanical efficiency and can be compared to fuel energy supplied to determine thermal efficiency. The term “indicated” implies a quantity measured from within the cylinder (originally on an indicator card) or a calculation made from such a measurement. Measurements at the flywheel or equations made from such measurements are called “brake” quantities.

- Pumping indicated mean effective pressure (PIMEP) is the fraction of NIMEP required to get air into and out of the engine. This is always a loss and can be very significant at moderate-to-light loads in a spark ignition engine.

- Fuel combustion rate can be calculated using the measured pressure and calculated volume in a first-law analysis. Combustion rate is used to assess effects of combustion chamber design effects on flame propagation and helps in efforts to optimize efficiency and minimize pollution emissions.

- Cycle-to-cycle variability and misfires that affects power, emissions, and drivability. By definition, variation from one cycle to the next implies that at least some of the cycles are not optimized. Since modern data-acquisition systems can measure a large number of consecutive cycles of pressure data, the variation can be accurately measured.

- Knock quantification. Knock is abnormal combustion caused by self-ignition of the charge prior to arrival of the normal flame front and degrades performance

and can destroy an engine. Even mild knock causes a very distinct oscillation on the cycle-resolved pressure, consequently cylinder-pressure measurements are the best way to detect and quantify its presence.

Cylinder pressure data can also provide a variety of engine control and performance information. Optimum spark timing, fuel-air ratio control, and charge temperature estimation are all available through the analysis of cycle pressure data.

Engine researchers have long noted the importance of pressure measurements in engine research. Until the 1950's, these data had to be taken over many cycles using mechanical indicator mechanisms (hence the association of the word “indicated” with cylinder-pressure measurements). With the innovation of the piezo-electric pressure transducer, individual consecutive cycle-resolved measurements became possible. This device contains a quartz crystal which emits a small charge when it is put under dynamic stress. Piezo-electric transducers are appropriate for cylinder-pressure measurement because they have a high frequency response, a small size, and accurate, linear response; however, during operation they are affected by thermal transients including thermal shock.[3]

Thermal shock is generated when rapid changes in temperature, caused by the arrival of the flame, vary the Young′s modulus and resonant frequency of the quartz crystal and cause the expansion or contraction of the diaphragm.[4] Thermal shock in combustion-pressure measurements has been shown to far exceed 50 kPa and affects the measurement through the exhaust stroke and into and sometimes beyond the intake stroke.[5] This error affects the accuracy of all the previously listed parameters of interest, under all engine-operating conditions. In particular, thermal shock makes the pumping process measurements useless at moderate-to-high engine load given that the error can be on the order of half the cylinder pressure during the intake and exhaust process. Manufacturers and users have expended significant effort to minimize the effects of thermal shock. These include coating the transducer diaphragm with silicon, in an attempt to damp rapid changes in heat flux at the diaphragm, designing the

transducer housing to compensate for thermal stress, and recess mounting the transducer. When recess-mounted, the transducer communicates with the cylinder through a single or series of passages which quench the flame prior to its impinging on the transducer surface. While some success has been achieved in reducing thermal shock effects, each of these solutions has practical limitations which leave thermal shock as a serious cylinder-pressure data quality issue. In particular, silicon coatings have limited life and reduce transducer frequency response and recess mounting can be affected by passage-transducer cavity resinous and passage clogging.[6]

TECHNICAL APPROACH

OVERVIEW

The objective of this work is to characterize engine combustion-pressure-measurement errors caused by flame-induced transducer thermal stress. A quantitative understanding of thermal shock is needed to facilitate mathematical models that can identify and remove thermal shock from measured pressures.

To characterize thermal shock error taken from pressure transducers within an engine, thermal shock must be quantified and correlated with prevailing engine conditions. This is difficult in an engine. Flame propagation and temperature vary spatially and from cycle-to-cycle and establishing a non-shocked reference measurement is challenging. Kistler Instruments, the leader in piezo-electric combustion-pressure-transducer technology, uses a large water-cooled transducer (model 7061) to provide a reference signal. Flame-induced rapid heating is damped by the large mass and water-cooling compared to smaller transducers. Unfortunately, the large size makes it difficult to mount in a modern, multi-valve combustion chamber and limits its frequency response. One of the objectives of this work is to determine if it is appropriate to use the 7061 as a thermal shock reference.

To solve the difficulties associated with quantifying thermal shock in a running engine, an atmospheric engine-flame simulator was built and used to characterize thermal shock behavior. The results from the simulator were then compared to engine measurements.

The engine-flame simulator used a chopper-wheel to intermittently impinge a high temperature flame on a pressure transducer and fast response thermocouple exposed to constant atmospheric pressure. The heat flux created by the flame was

calculated using the thermocouple. Any change in the pressure transducer's output is attributed to thermal shock since the prevailing pressure was constant. The pressure transducer's response to the flame revealed a relationship between the thermal shock error and the heat flux through the transducer.

The thermal shock error within the engine was characterized using two simultaneously acquired pressure measurements. One measurement was acquired with a transducer that was exposed to combustion gases throughout the engine cycle, and the other was taken with a transducer mounted lower in the cylinder. This transducer was protected by the piston until the flame had extinguished and was therefore not subjected to thermal shock. The difference between the two measurements was due to the thermal shock error. The measurements were made at several engine-operating conditions to verify that the engine-flame simulator's test conditions did in fact simulate in-cylinder conditions and to attempt to establish a relationship between engine heat transfer and thermal shock.

EXPERIMENTAL APPARATUS AND PROCEDURES

This subsection provides detailed descriptions of the engine-flame simulator design and use, the engine modifications, data acquisition procedure necessary to acquire in-cylinder thermal shock data, and the calibration procedures for the critical transducers and instrumentation.

ENGINE FLAME SIMULATOR

The following describes the design and operation of the engine-flame simulator (EFS).

The purpose of the EFS is to simulate thermal shock on a pressure transducer by intermittently exposing the transducer to a high temperature flame while maintaining ambient atmospheric pressure. To accomplish this, a flame from an oxygen-acetylene torch was chopped with a slotted rotating disk (pictured in Figure 2). The steel disk rotates and the solid portions of the disk block the flame while the flame passes through the slots in the disk. The flame impinges on a pressure transducer and a fast response thermocouple that are mounted in an aluminum housing. The housing is shown in Figure 3. The transducer is exposed to constant atmospheric pressure; therefore any change in its output is attributed to thermal shock.

The EFS is constructed from aluminum with a Dayton 3-phase inverter duty motor that powers an 18-inch steel flame chopping disk. The steel disk has two 1-inch wide slots extending radially for 6 inches. A Victor model 65428 oxygen-acetylene torch is clamped to a fixture that was designed to slide on two horizontal bars mounted on the side of the wheel opposite the transducer. The torch flame aligns with the transducer and thermocouple. This torch head was chosen for a wide flame-front to strike evenly on the transducer and thermocouple. The transducer housing holds either a Kistler type 6125 or 7061(shown in Figure 4 and 5) pressure transducer and a Nanmac fast-response thermocouple (shown in Figure 6). The pressure transducer signal goes to a Kistler type 5010 charge amplifier. The thermocouple signal is amplified using a Preston 8300 XWB amplifier. These signals are fed into a Superflow ICEADAQ data acquisition and combustion analysis system. A Heidenhain R00426B incremental shaft encoder coupled to the chopper disk synchronizes the measured data and the disk's angular position. The encoder sends out one signal every 0.5 degrees rotation of the disk (720 times per revolution) and sends out an additional signal once each revolution. The once-per-revolution signal initiates the data acquisition, while the 0.5 degree signal is used as an acquisition timer for the process.

The procedures for operating the thermal shock wheel focus primarily on operator safety and data accuracy. Two people operate and take data from the wheel.

The torch was lit off to the side of the wheel and the flame was calibrated to a specific and repeatable temperature using a k-type thermocouple mounted 18 inches from the torch head. The temperature was controlled by adjusting oxygen-to-acetylene ratio as well as total flow rate. The motor was set at the test speed with a digital motor-speed controller and the torch aligned with the transducer and thermocouple.

Initial results were invalid because the motor emitted a high-level electrical noise that interfered with the signal. To correct this problem, the wheel speed was increased above the desired level, and the motor turned off while the wheel was allowed to coast. Data acquired with the wheel coasting, avoided the motor-generated noise. This technique resulted in data variations around 50 RPM for a given test. The effect of varying RPM subsequent analysis was accounted for by using the instantaneous wheel speed that was recorded for each revolution.

TEST ENGINE

The following describes the engine modifications necessary to acquire signals to verify EFS results and the engine experiment test set-up and procedure.

Engine Modifications

This section provides a general overview of the engine modifications that were made in order to take pressure and temperature measurements from three locations within a cylinder. The general specifications for the test engine are provided in Table 1. An Intelligent Controls IC 45460 engine management system was used to control the fuel injection and spark timing.

TABLE 1:Engine Specifications for Test Engine

Manufacturer	General Motors
Model	LT1 V-8
Year	1992
Displacement	5.7 L
Bore	10.16 cm
Stroke	8.84 cm
Compression Ratio	8.91:1
Firing Order	1-8-4-3-6-5-7-2

A test engine was modified to accommodate three transducers and a fast response thermocouple into a single cylinder. Following the work of Puzinauskas to measure pressure drops across intake valves and to measure absolute cylinder pressure, a Kistler 4045 piezo-resistive transducer is located 3.5 inches down the wall of the cylinder. The modification is pictured in Figure 7. In this work, the placement was chosen so that this transducer would not be exposed to combustion gases until after the flame had extinguished, thereby protecting this transducer from thermal shock. This particular transducer model was chosen for its accuracy; however, it is not capable of withstanding temperatures higher than 150 degrees Celsius. To minimize the chance of overheating the transducer, a special housing had to be built to cool the transducer while maintaining contact with the cylinder wall. This adaptor, as pictured in Figure 8, holds the transducer against the cylinder wall with a spring-loaded mount, which allows for the thermal expansion of the cylinder. The tip of the adaptor has a set of four holes that match those at the cylinder wall. There are two 3 mm holes and two 2 mm holes. The size and pattern of these holes were chosen to maximize the resonant frequency of the passage-cavity system to prevent distortion of the measured signal as described by Puzinauskas[7].

One head was modified, as shown in Figure 9, to allow flush-mounting a Kistler 7061 transducer in the combustion chamber. A separate tap is located 8 mm from the transducer to accommodate a fast response thermocouple.

Engine Test Set-up and Procedures

Operation of the test engine was designed to make the retrieved data as repeatable as possible. The first step was to allow the engine to warm-up. Typically, this warm-up period lasted until the engine oil temperature was above 125 degrees Fahrenheit. During this period of warm-up, the engine operator manipulated the engine controls to achieve the desired fuel-to-air ratio. After the engine had been warmed up, the desired load and engine speed were placed on the engine by the engine controls. The data acquisition system was activated once the desired engine operating parameters had been achieved.

CALIBRATION

The following describes the calibration of the pressure transducers and fast response thermocouples used in this study.

Pressure Transducers

Pressure transducer calibration was performed to measure any differences in output between the transducers for a known pressure. This was essential given that the nature of the project was to minimize combustion cylinder-pressure measurement error and was particularly important for the engine data, in which comparisons were made between two transducers simultaneously measuring the same signal. Two types of transducers were used in this investigation; piezo-electric transducers, which are the primary object of this effort, and piezo-resistive transducers, which were used as the low-pressure reference, during engine testing. Piezo-electric transducer signals naturally decay over time and are therefore only suitable for dynamic measurements like engine cylinder pressure measurements. Consequently, they must be calibrated using a dynamic procedure. Piezo-resistive transducers are similar to strain gauges and

can therefore be calculated with a static procedure. Their procedures are described in the following subsections.

Static Calibration

The Kistler type 4045 piezo-resistive pressure transducers, shown in Figure 10, were calibrated using a standard dead weight tester to create a known static pressure. The dead-weight tester generates the known pressure by hydraulically lifting precise weights with a piston with an accurately known cross-sectional area. Under static conditions the pressure in the hydraulic fluid is uniform and equal to the lifted weight divided by the piston area. A fixture is inserted in the hydraulic line where transducers can be mounted and exposed to this pressure. The transducer was installed in the dead weight tester fixture and then subjected to the known pressure. A Kistler piezo-resistive amplifier was used to provide excitation current to the transducer and amplify its output. The output was recorded using a 4-½-digit voltmeter. Pressures were applied to the transducer in 50 psi intervals from 50 to 300 psi. At each pressure, ten measurements were taken. These output voltages were averaged and then graphed against the applied pressure. The output voltage versus the applied pressure formed a linear function and the slope of this provided the necessary calibration data for the transducer. Three 4045 pressure transducers were calibrated using this technique. Typical results are shown in Figure 11. The linearity and repeatability of each transducer and amplifier combination was better than 0.5%.

Dynamic Calibration

Both the Kistler type 6125 and 7061 piezo-electric transducers were calibrated using a dynamic variation to the above technique. The charge output signal of these transducers was input to a charge amplifier via a high-impedance cable. The charge amplifier converts the low level charge (which is of the order of several Pico-Coulombs) to a proportional voltage, which can be recorded with standard data

acquisition equipment. In this procedure, a known pressure was applied to the transducer. Then the output was grounded to zero volts, thereby eliminating signal decay. The pressure was then abruptly dropped to atmospheric by rapidly releasing the hydraulic pressure holding up the weights and allowing the weights to fall. The resulting voltage change was recorded as a function of time using a digital oscilloscope programmed to trigger on a voltage drop. The voltage change caused by the pressure change was determined using a peak-to-peak calculation feature on the scope. Dynamic pressures were taken at intervals of 200 psi from 200 to 1000 psi. Ten measurements were taken at each dynamic pressure. These were then averaged and then graphed against the corresponding voltage output. Three 6125 and one 7061 transducers were calibrated and the sensitivity of each transducer determined. Figures 12 and 13 show the results for this procedure. The linearity of all four transducers was better than 1%. Repeatability was about 2 to 3%. The non-repeatability was more likely due to dynamic procedural effects such as piston friction and pressure oscillations in the hydraulic fluid.

Fast Response Thermocouples

Overview

The purpose of the fast response thermocouples was to enable calculating the approximate heat flux through the transducer associated with the flame-induced thermal shock error. The thermocouples provided combustion chamber surface temperature, which can be used to calculate heat flux. The heat flux calculation is described in the next subsection. For both engine and EFS tests, 1/8 inch diameter eroding-type fast-response thermocouples were used. These thermocouples have an aluminum pin with a stainless steel housing. These thermocouples have their parallel chromel and alumel wafers separated by insulating material running down the center of the aluminum pin. A very fine junction is made on the thermocouple surface by “eroding” the aluminum with fine-grit sand paper. The voltage output of the junction is actually proportional to the eroded aluminum particles that bridge the gap across the insulation wafer. The

thermocouple's response is inversely proportional to the size of the eroded particles and is on the order of milliseconds when using 400 grit sandpaper. In addition to this fast response, this construction allows contouring the thermocouple surface to match the engine combustion chamber.

As is evident from the heat transfer calculation description, converting the temperature output to heat flux requires knowledge of the thermal properties of the thermocouple material. Because several different thermocouples were used in this project, it was necessary to establish each thermocouple's thermal properties.

Calibration

The technique described by Gatowski was followed in this work[8]. An apparatus was constructed which held a high-intensity lamp that was used to irradiate a perpendicular aluminum surface with a constant heat flux. The fast-response thermocouple was mounted flush in the surface in order to measure the transient surface temperature. This apparatus is shown in Figure 14. The fixed heat-flux was repeatedly exposed to the aluminum/thermocouple surface, and the transient surface temperature data was recorded using a digital oscilloscope programmed to trigger on rising voltage.

The necessary thermocouple thermal-properties required to calculate heat flux are thermal diffusivity (α) and thermal conductivity (k). The thermal diffusivity stays relatively constant despite voids and gaps in the construction, because the effects of such imperfections would similarly decrease the values of the terms in both its numerator and denominator. The value of the thermal diffusivity can therefore be estimated from a handbook with reasonable accuracy.

The procedure described herein provides a quantity β defined by:

$$b = \sqrt{krc} \qquad \textbf{EQN 1}$$

If α is assumed known, k can be determined by combining equations.

$$k = b * a^{1/2} \qquad \textbf{EQU 2}$$

The square root dependence on α further justifies the handbook value assumption and the equation above shows that determining β essentially determines k.

If the thermocouple is assumed to be semi-infinite, a theoretical response to constant heat flux dependent on β, the elapsed time, and the magnitude of the heat flux can be formulated by solving heat conduction equation. In this case, the boundary conditions are prescribed in terms of the spatial derivatives of the temperature, which are determined by the known constant heat-flux on the surface and the assumption of the infinite depth. The thermocouple is initially assumed to be at constant temperature. The solution is best obtained by the Laplace-transform method and results in a time and spatially resolved temperature distribution. When evaluated at the thermocouple surface, this solution gives the theoretical response of the surface to a known heat flux:

$$T_{THEORETICAL}(t) = \frac{2q_0}{b}\left(\frac{t}{p}\right)^{1/2} \qquad \textbf{EQN 3}$$

By minimizing the least-squares error between the theoretical and measured responses, a best value for β can be established. The thermal conductivity values determined for the thermocouples used in this project are shown in Table 2.

Table 2: Beta values for two thermocouples

	β [J/m^2*K*sec$^{1/2}$]
Thermocouple 1	24198
Thermocouple 2	21052

DATA REDUCTION AND ANALYSIS

The following subsections describe the methods used to quantify thermal shock from the experimental data in both the EFS and the engine and to calculate heat flux from measured surface temperature.

THERMAL SHOCK QUANTIFICATION

Engine Flame Simulator

Thermal Shock created with the EFS was quantified by calculating the difference between the pressure signal just before the shock took place and the maximum deviation from this after the flame contacted the transducer. Because the test was performed in open atmospheric conditions, the sharp drop in the pressure curve can only be attributed to the thermal shock caused by the impingement of the flame.

Engine

Because of the dynamic pressure conditions found within an operating engine cylinder, a separate method for determining thermal shock had to be developed. The piezo-electric transducer being tested was installed in the head of the engine so that it would be exposed during the whole cycle of the engine. A piezo-resistive pressure transducer was placed mid-way down the length of the cylinder. This transducer is protected from the combustion flame associated with hot gases because the piston covers it until the combustion process is complete. Consequently, this transducer is protected from thermal shock. Thermal shock can then be quantified, when the lower pressure transducer is un-covered and both transducers are exposed to the cylinder pressure, by calculating the difference between the outputs of the two transducers. Because the low-pressure transducer is not uncovered until some time after the flame impinges on the full cycle transducer, the calculated pressure difference only represents the thermal shock after some recovery has already occurred. While this is not ideal, it

does indicate the thermal shock level during parts of the gas exchange process. This is believed to be where the thermal shock effects are among the most severe.

HEAT FLUX CALCULATION

The surface heat-flux is calculated from the temperature data recorded by the fast response thermocouple. The technique used to carry out these calculations has been described in detail by Puzinauskas[9]. A brief summary is included here for completeness.

The conduction equation for one-dimensional heat flow in the wall of a semi-infinite solid with constant material properties is,

$$\frac{\partial T}{\partial t} = a \frac{\partial^2 T}{\partial x^2} \qquad \textbf{EQN 4}$$

where

$$a = k/(rC) \qquad \textbf{EQN 5}$$

This equation is linear; therefore the solution can be decomposed into a steady state and transient component. Since it is believed the transient portion of the heat flux is the primary cause of thermal shock, the steady state solution was ignored.

Two boundary conditions are required for the solution. The first comes from the measured surface temperature, which is represented with a Fourier series. The second is obtained by assuming that the temperature gradient within the wall beyond the penetration depth of the heat flux is equal to zero.

The solution, obtained by separation of variables, is:

$$T_{transient}(x,t) = \sum_{n=1}^{\infty} e^{-xr}\left(A_n \cos(nwt - xr) + B_n \sin(nwt - xr)\right) \qquad \textbf{EQN 6}$$

where A_n and B_n are coefficients of the Fourier series obtained from the surface temperature boundary condition. Evaluating the spatial derivative of the temperature solution at the wall and using the result in Fourier's Law of Conduction obtain the heat flux:

$$q_w = -k\sum_{n=1}^{\infty} r\{(A_n - B_n)\sin nwt - (A_n + B_n)\cos nwt\} \qquad \textbf{EQU 7}$$

RESULTS

ENGINE FLAME SIMULATOR RESULTS

First, the test matrix is provided. Next, an explanation of the cycle-resolved data and a detailed examination of a single test point are presented in order to establish data accuracy. Finally, the results of the various test points enumerated on the EFS test matrix are presented.

ENGINE FLAME SIMULATOR TEST MATRIX

Five test points taken on the thermal shock wheel were measured with the Kistler type 6125 pressure transducer and the fast response thermocouple combination. The rotational speed of the slotted disk was varied as well as the temperature of the impinging flame.

Table 4: Test Matrix 1

	1800 RPM; 500 F Wheel test 1	
1400 RPM; 300 F Wheel test 4	1400 RPM; 500 F Wheel test 2	1400 RPM; 700 F Wheel test 5
	1000 RPM; 500 F Wheel test 3	

Five test points were measured with the Kistler type 7061 pressure transducer and the fast response thermocouple combination. The 7061 transducer was operated with cooling water. The rotational speed of the slotted disk was varied as well as the temperature of the impinging flame.

Table 5: Test Matrix 2

	1800 RPM; 500 F Wheel test 6	
1400 RPM; 300 F Wheel test 9	1400 RPM; 500 F Wheel test 7	1400 RPM; 700 F Wheel test 10
	1000 RPM; 500 F Wheel test 8	

Five test points were measured with a combination of two thermocouples. This was done to measure any difference in heat flux between the original position of the pressure transducer and the thermocouple. The rotational speed of the slotted disk was varied as well as the temperature of the impinging flame.

Table 6: Test Matrix 3

	1800 RPM; 500 F Wheel test 13	
1400 RPM; 300 F Wheel test 16	1400 RPM; 500 F Wheel test 14	1400 RPM; 700 F Wheel test 17
	1000 RPM; 500 F Wheel test 15	

CYCLE-RESOLVED DATA

Figure 15 shows the cycle resolved thermal shock and heat flux for a test on the EFS. The figure displays the pressure output of the transducer at the beginning of the cycle. It is important to note that the thermal shock simulator tests were all performed at atmospheric conditions, so without any thermal shock the pressure output should be constant. The figure shows pressure signal is increasing as it recovers from a previous shock, until it is shocked again. As the flame impinges upon the transducer, an erroneous pressure output is created, and the pressure trace drops sharply 7.5 kPa.

This drop perfectly illustrates thermal shock. As the flame is removed from the transducer housing, the transducer begins its subsequent recovery.

DETAILED EXAMINATION OF A SINGLE TEST POINT

The data analysis allows several different graphical presentations that can be used to characterize the data and the associated error. Each of these and the significant information they contribute are discussed below. The results of these are associated with test from the test matrix.

Individual Cycle Analysis

At each test point, four graphs shown in Figures 16 - 19 were plotted that show the relationship between the following: The change in temperature versus the resulting thermal shock, the change in heat flux and the resulting thermal shock, the location of maximum temperature difference and the resulting location of the maximum thermal shock, and the location of the maximum heat flux and the resulting location of maximum thermal shock. Figure 16 shows significant variation in both thermal shock and temperature (pulse). Variations of 10 kPA in thermal shock and variations of 3 degrees temperature difference are seen when conditions were expected to be more repeatable from cycle to cycle. Figure 17 shows the change in heat flux and the resulting thermal shock for the same test. The results are similar to Figure 16. The uncertainty in this graph is up to 1.5 MW/m^2.

Figures 18 and 19 as well illustrate variation in the crank angle location of peak temperature pulse and the location of peak thermal shock. The location of the maximum temperature occurs over a 15-degree range while the location of the maximum thermal shock occurs over a 40-degree range. Because the flame path to the transducer and thermocouple is exposed at exactly the same moment in each cycle and this moment is accurately known from the encoder output, it is expected that variations

are caused by cycle-to-cycle and spatial variations of the flame. This is investigated further in the next section.

Spatial Heat Flux Variations

The thermal shock simulator was intended to create a repeatable, intermittent heat flux to shock the pressure transducer, which could be quantified by the adjacent fast-response thermocouple. An oxygen-acetylene torch was chosen to generate a flame-induced heat flux because this was assumed to be similar to a flame occurring in a firing engine cylinder.

As seen in Figure 3, the face of the transducer and the tip of the thermocouple had to be separated a distance of 15 mm to allow the transducer and the thermocouple to be threaded into the back of the housing. Because of this separation, the exact heat flux at the face of the transducer could not be known because of the horizontal separation distance between the transducer and the thermocouple.

To determine the effect of this separation distance, flame-exposure tests were performed with a second thermocouple mounted in place of the pressure transducer. This test quantifies the flame impingement differences between the pressure transducer and thermocouple locations during the shock rig tests

Figures 20 and 21 show results from simultaneous thermocouple measurements taken from 50 consecutive cycles with the wheel rotating at 500 RPM and a flame temperature of 1400° F. Were the flame repeatable from cycle to cycle and between locations, the data on Figures 20 and 21 would appear as a single dot with equal x and y values. If cycle-to-cycle variation were significantly higher than the spatial variation, the data on these graphs would be linear with a unity slope. These situations would be desirable, because they would imply a high level of significance to each cycle's result and minimize the need to analyze a large number of cycles. As is evident from Figures 20 and 21, this was not the case. Instead, the figures indicate a large amount of scatter

between the two thermocouple locations, indicating the spatial variations within the flame were on the order of the cycle-to-cycle variations.

The flame emitted from the torch was observed to be turbulent and unsteady. This fact coupled with a rotating wheel that disturbed the air with separation gradients and eddies, explain the spatial variations that were observed in the heat flux of the flame.

One noteworthy aspect of this data is that averaging over many cycles, the average of the calculated heat flux pulses at the two locations only varied by 12 %. The 20% difference in the average temperature pulse under conditions where the average heat flux pulse is so close is attributable to the 13% lower thermal conductivity revealed during the calibration process. Examination of Equation 7 shows how a lower thermal conductivity would yield a larger temperature pulse for a given heat flux. Figures 22 and 23 show the ensemble-averaged, cycle-resolved temperature and heat-flux histories for both thermocouples. These figures also indicate similar heat transfer resulting from noticeably different temperature histories. While the transient temperature histories of the two thermocouples are different, the steady state temperatures are only about 4°C different. This difference, which is on the order of the pulse magnitude, can also be explained by the lower thermal conductivity of thermocouple two given that it is the warmer of the two.

Statistical examination of the spatial variation of the heat flux pulse shows that the coefficient of the variation is about 8% and that for the temperature is about 17%. This is similar to the cycle-to-cycle variation of heat flux seen in the thermal shock test results indicated by figures 16 and 17. This suggests that the spatial flame variation is a significant source of the variation in the thermal shock testing.

The implication of these results is that because the spatial variations average out over many cycles but are significant in individual cycles, appropriately averaged data must be used to draw conclusions from the results of this study. Additionally, surface temperature measurements recorded from a temperature probe separated from the pressure transducer cannot be used to correct individual-cycle thermal shock error.

EFFECT OF HEAT FLUX LEVEL AND EXPOSURE TIME ON THERMAL SHOCK MAGNITUDE AND RECOVERY

This subsection discusses the results from the EFS test matrix using the 6125 transducer. These results were examined for a relationship between thermal shock magnitude, temperature, and heat flux pulse in order to characterize the thermal shock process.

Effect of Thermal Shock Magnitude

Figures 24 and 25 show thermal shock versus temperature pulse and heat flux pulse, respectively. Each test contains 50 consecutive cycles of data. These 50 cycles were averaged and then statistically analyzed to calculate variation. This variation is indicated by the error bars on the figure, which correspond to plus and minus one standard deviation of the average. The figures indicate a nearly linear relationship between thermal shock and both temperature and heat-flux pulse, although of the two, the correlation between thermal shock and heat-flux pulse is much more clearly linear. Consequently, heat flux appears to be the more accurate correlation variable for a potential thermal shock correlation model. It would be desirable if the temperature could be the correlation variable with the thermal shock, because then the relatively computationally intensive heat-flux calculation could be avoided.

A second advantage of the heat flux over the temperature is that it inherently accounts for variation in thermocouple thermal conductivity with its calculation. This advantage is not illustrated here, because all the data were acquired using the same thermocouple, but, if a thermocouple had to be replaced, some scheme would have to

be developed to account for possible variation in conductivity. As was discussed in the29 flame signal variation section, lower thermal conductivity results in larger temperature pulses for a given heat flux.

Characterization of Thermal Shock Recovery

Based upon the first law solution of the temperature at a uniform solid cooling in an ambient fluid, it was initially hypothesized that the recovery of the transducer from thermal shock would be a purely exponential function. To confirm or disprove this recovery behavior, cycle-resolved EFS pressure measurements were analyzed at the point of thermal shock until its recovery.

Because of the cycle-to-cycle variations in peak and location of peak thermal shock discussed previously, an ensemble average pressure trace using of all 50 cycles measured would not have been a very good representation of what was happening to the pressure transducer. The peak thermal shock would be "smeared" during averaging because of the variation in the crank angle location of the peak. When the peak thermal shock location of one cycle occurs at a different crank angle location than another cycle it is averaged with, the two cycle peaks will be averaged with points off the peak in the ensemble average. The result is that the peak thermal shock of the ensemble average will be significantly lower than the average of the individual cycle peaks. If the data were perfectly noise-free, the solution would be to examine a single cycle. Because of the noise, a "conditioned" ensemble average is used instead. To create this conditioned ensemble average pressure trace, cycles within a test, which did not have similar peak and locations of peak thermal shock, were discarded. The remaining values were then averaged to create a representative ensemble average.

Figure 26 and 27 show conditioned, cycle-resolved, ensemble averaged thermal shock curves generated by average heat fluxes of and MW/m^2, respectively. The signal shown in Figure 26 contains much more noise than Figure 27 does because of the limited resolution relative to the smaller thermal shock values. Despite the

additional noise, the recovery behavior is similar in both cases. In both cases the pressure trace is exposed to a heat flux and the pressure output of the transducer drops. After thermal shock takes place, the transducer begins its recovery and this recovery contains both linear and exponential components

Analyzing the previously mentioned Figure 15, the recovery appears to contain both linear and exponential components. The pressure trace recovers to a level above the value when it was shocked. This is normally associated with long-term thermal drift, which is caused by the over-all heating of the transducer. Long-term thermal drift has traditionally been ignored, because it was not believed to be significant within a single engine cycle and can be easily fixed cycle-to-cycle by pegging the value of the pressure transducer signal at the beginning of each cycle to a known pressure. This known pressure can be measured or estimated using the manifold pressure or other analytical methods[10].

Effect of Transducer Mass and Water-Cooling on Thermal Shock

To examine the effect of transducer mass and water-cooling, the tests described above were performed on a Kistler 7061 pressure transducer with and without water-cooling. Figure 28 shows a photograph of the 7061 next to the 6125. The 7061 has a 14 mm diameter compared to the 5 mm diameter of the 6125. The tubes leading behind the 7061 are to supply and return cooling water to the transducer.

Kistler often compares data from their more practical (e.g. 6125) transducers to that simultaneously obtained from the 7061 to characterize the thermal shock behavior of the smaller transducers. The resulting data from these investigations show that although the 7061's thermal shock is an order of magnitude smaller than the 6125's thermal shock experience, it still exists. Because it is about 10 times smaller though, using the 7061 as a thermal shock baseline for the 6125 is appropriate. Although the 7061 pressure transducer has minimal thermal shock effects, it is impractical for in-

cylinder pressure measurements because of its large size, especially in constructed combustion chambers of modern multi-valve automotive engines.

Five tests were performed on the 7061 transducer as described by the test matrix and the results were averaged and then statistically analyzed. The results are plotted on Figure 29, which shows that the 7061 experiences a different relationship between thermal shock and temperature than does the 6125. The relationship is not linear and appears to reach a maximum point of thermal shock near 2 degrees of temperature change.

Analysis of the cycle resolved ensemble average of the pressure trace, illustrated in Figure 30, shows that the 7061 recovers from thermal shock in a different manner that the 6125. The recovery appears to have a linear and an exponential component, like the 6125, but the exponential component is much smaller, and the linear component has a negative slope. Since the exponential recovery increases the pressure while the linear recovery decreases, the pressure actually displays a maximum between thermal shock events.

A large factor in the reduction of the thermal shock effects on the 7061 pressure transducer is the fact that it is water-cooled. As pictured in Figure 5, the 7061 transducer is housed in a moving water jacket. This water practically eliminates long-term thermal drift and greatly reduces thermal shock. An interesting phenomenon occurs as a result of this water flow. From plots taken from the EFS with the 7061 transducer housing, it is seen that at the moment of flame arrival a sharp peak in the pressure curve occurs and then disappears. Although this momentary peak does not degrade the overall data output from the transducer it is interesting to note. A possible reason for this occurrence is that the heat flux causes a rapid boiling of the water at the diaphragm of the transducer and then quickly disappears as the flowing water compensates for this increase in heat.

Although the reason for the sharp pressure peak and then recovery in the 7061is unknown it can be used for the purpose of locating the moment of flame arrival at that

location. This peak could possibly be used as a trigger for any thermal shock-correcting factor.

ENGINE RESULTS

Figure 32 depicts the cycle-resolve heat flux for two engine-operating conditions. The solid line represents the averaged trace of the 50 consecutive cycles. As previously described in the EFS data results, the 50 cycle average caused a smearing effect on the data at its peak because each cycle has a slightly different location of maximum heat flux. The maximum heat flux calculated by averaging the maximum of each individual cycle is represented by the dot on the graph. The maximum heat flux for the average maximums is higher than that of the ensemble average because of the smearing effect caused by variation in the crank-angel location of the peak heat flux.

The maximum heat flux occurs at approximately 220 degrees of crank angle. This point is well after cylinder ignition because of the time that it takes the flame to arrive at the location of the thermocouple.

The figure also shows the peak heat flux is higher in the lower speed engine condition than the higher speed engine condition. This was caused because the engine spark timing was held constant for all tests, even when the engine speed was increased. As engine speed is increased, optimal ignition timing occurs earlier in the cycle to give the flame time to propagate across the combustion chamber in a shorter cycle time. Consequently, the spark timing was late for the faster speed, and therefore the heat release occurred late in the expansion stroke. This resulted in significantly lower peak pressure and temperature in the higher speed case. The lower temperature resulted in a lower peak heat flux magnitude. This is illustrated by the ideal gas temperature

calculation made from the measured full cycle pressure shown in Figure 33. As the cycle reaches the exhaust phase, the air in the faster test cycle is higher in temperature than that in the slower engine test cycle. This higher temperature gas, coupled with the faster moving air, greatly increase the co-efficient of heat transfer during the exhaust phase for the higher speed cycle. The heat flux magnitude shown in this figure verifies that the heat flux magnitude created on the EFS were representative of those experienced within the engine.

Figure 33 shows the pressure versus crank angle for an individual engine condition. The high-pressure transducer trace experiences the whole cycle of cylinder pressure and is therefore affected by thermal shock. At approximately 90 degrees the piston covers the low-pressure transducer. As the piston begins to compress the air-fuel mixture, the high-pressure trace starts to climb. Near the top-dead-center, the spark plug ignites the mixture and the temperature and pressure of the mixture rapidly increase. At the point marked by the vertical line, the heat flux at the location of the thermocouple reaches its maximum, and the pressure transducer is thermally shocked. The piston uncovers the low-pressure transducer and as seen in the graph the two pressure traces do not lie on each other. This is because of thermal shock. At this point, thermal shock can be quantified when it is referenced to a transducer that is not shocked.

Figure 34 highlights the thermal shock recovery process within the engine. The thermal shocks for two different engine speeds are displayed by subtracting the full cycle signal from the reference signal. The trace is non-continuous, because thermal shock cannot be measured within the engine when the piston covers the low-pressure reference transducer. It is important to note that the maximum thermal shock cannot be measured because the piston covers the reference transducer at the moment of thermal shock.

Figure 34 illustrates the effect that load and engine speed have on the thermal shock. The low speed tests have a higher maximum heat flux because of the reason described above. Higher engine speeds, however, do seem to cause a higher level of

thermal shock. This is related to the recovery time of the transducer. The faster engine operating condition does not allow as much time for the transducer to recover from the thermal shock at the point the reference transducer is uncovered. The result here is that, even though the maximum thermal shock of the higher speed case was likely lower than the lower speed case, the reduced recovery time caused the thermal shock at to be nearly equal.

By looking "across" the portion of the cycle where the reference transducer is covered during the end of the exhaust and beginning of the intake stroke two things are evident. First, it is clear that the transducer has not had time to complete its recovery in the high-speed case, while it seems to have reached a stable recovery at low speed. The positive slope at the start of compression draws this conclusion. The positive slope in this difference plot indicates the level of the full cycle transducer is rising relative to the reference, i.e., still recovering.

A second interesting feature this graph shows is that a recovery model appears possible. This would be accomplished by applying knowledge of the thermal shock recovery characteristic given in the EFS testing to create an analytical function, which would connect the signal curves across the portion of the cycle where the reference transducer is covered.

CONCLUSIONS AND RECOMMENDATIONS

1. Uncertainty is created by a combination of cycle-to-cycle and spatial variability in the flame of the oxygen-acetylene torch. This uncertainty makes characterization of the local heat flux difficult using a sensor remote from the location of interest. Therefore, a level of uncertainty must be expected when attempting to establish a relationship between heat flux and thermal shock using individual cycle data. The data produced by the EFS contained 20% spatial variation. This uncertainty should be eliminated if a repeatable head flux source is used (such as a high intensity lamp). This would allow removing the

transducer and measuring the heat flux at its exact location then replacing the transducer and exposing it to a precisely known heat flux.

2. A heat flux measurement used as an input to a model intended to remove the thermal shock error, is a measurement that should be made as close to the transducer as possible. In fact, best results would be obtained by integrating the heat flux sensor with the transducer.

3. The magnitude of thermal shock induced by an atmospheric flame for the industry standard pressure transducer (Kistler 6125) correlates linearly with the magnitude of rapid temperature change and linearly with rapid change in heat flux. The heat flux correlates better, because it is less affected by secondary flame pulsations, these have a less dramatic effect on the pressure transducer than the initial pulse.

4. Qualitative observations of transducer thermal shock recovery made from the EFS results indicate the recovery seems to be composed of a linear component associated with the thermal drift behavior to magnitude of impinged heat flux.

5. Engine thermal shock measurements showed that at 2400 RPM thermal shock caused by a 1.5 MW/m^2 peak heat flux does not recover within one engine cycle. This indicates that today's state of the art miniature pressure transducers still suffer large errors relating the thermal shock.

6. The Kistler 7061 pressure transducer was affected by thermal shock; however it experienced 85% less thermal shock than the 6125 transducer making the 7061 a good reference transducer when quantifying thermal shock in an engine.

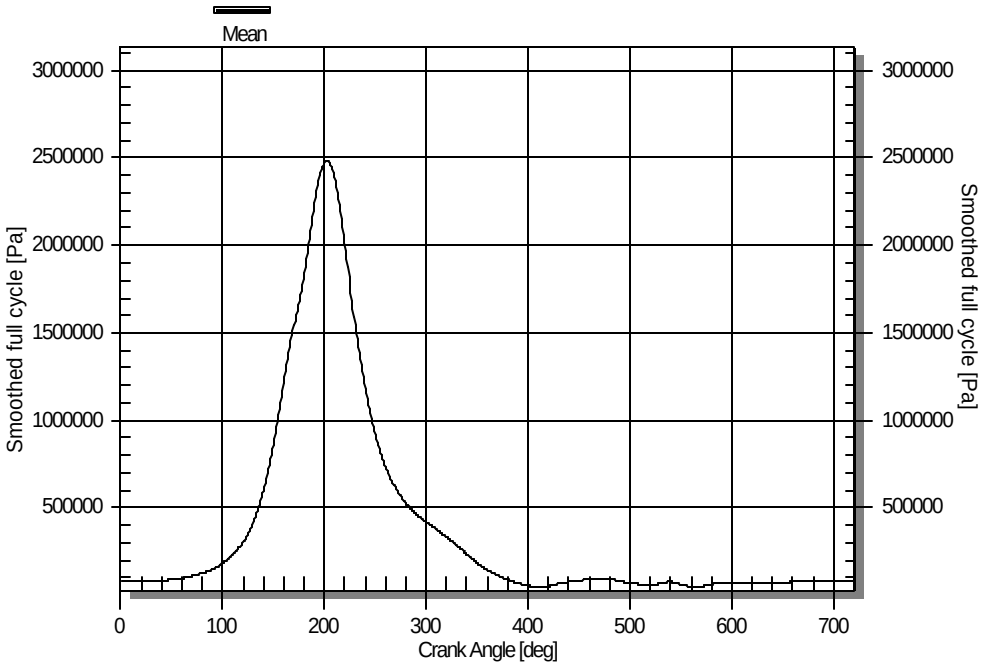

FIGURE 1a: Cycle Resolved Combustion Pressure vs. Crankshaft angle

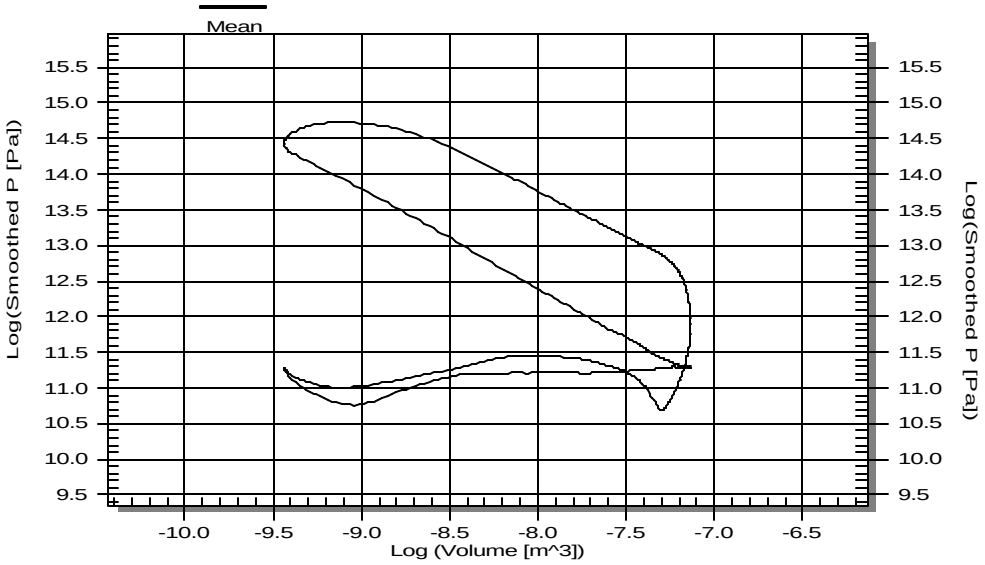

FIGURE 1b: Cycle Resolved Combustion Log Pressure vs. Log Volume

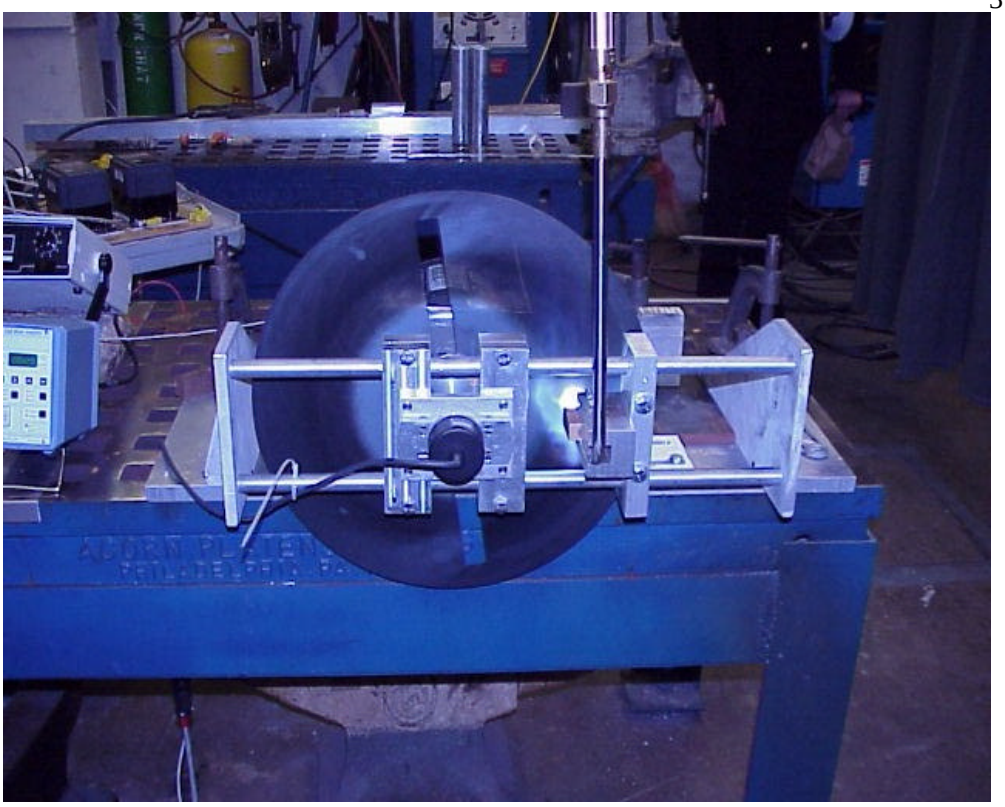

FIGURE 2: Engine Flame Simulator in Operation

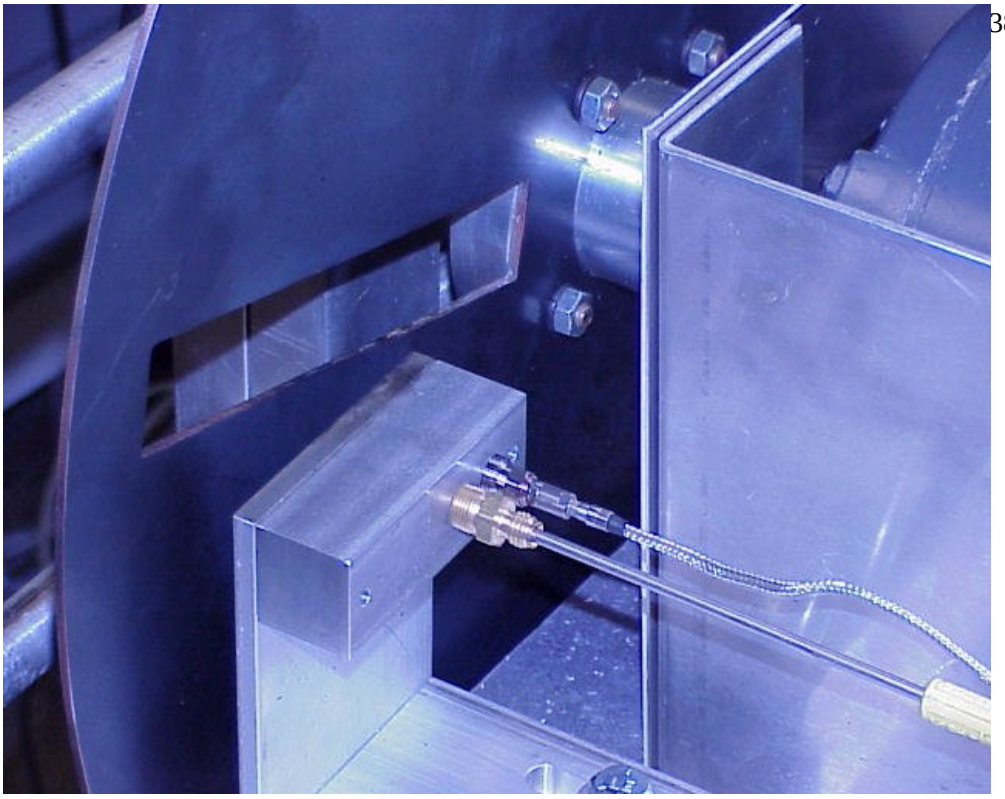

FIGURE 3: Transducer and Fast Response Thermocouple Housing

FIGURE 4: A Kistler 6125 Piezo-electric Pressure Transducer

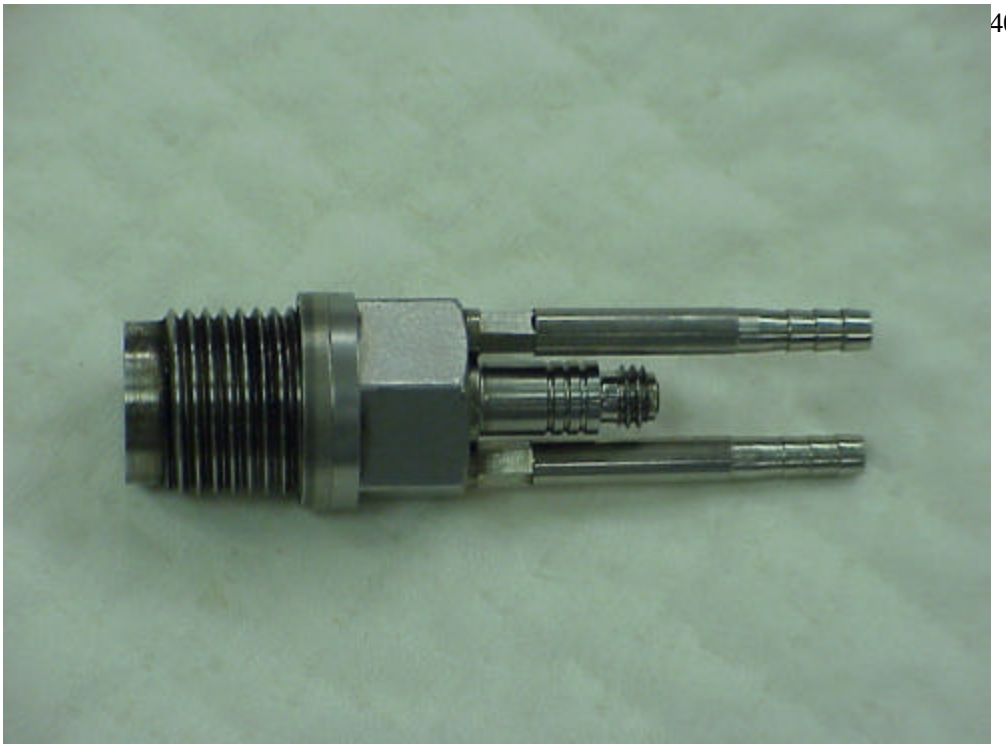

FIGURE 5: Kistler 7061 Piezo-electric Pressure Transducer

FIGURE 6: Nanmac Fast-Response Thermocouple

FIGURE 7a: Engine Modifications to Allow Low-Pressure Transducer Access

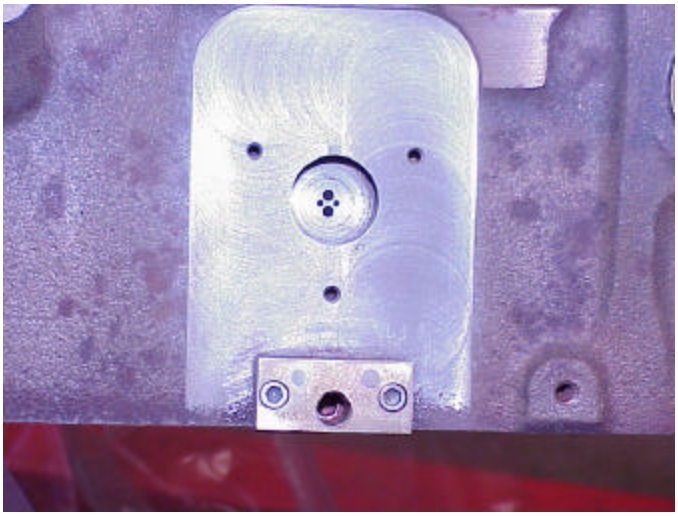

FIGURE 7b: Engine Modification for Low-Pressure Transducer (close-up)

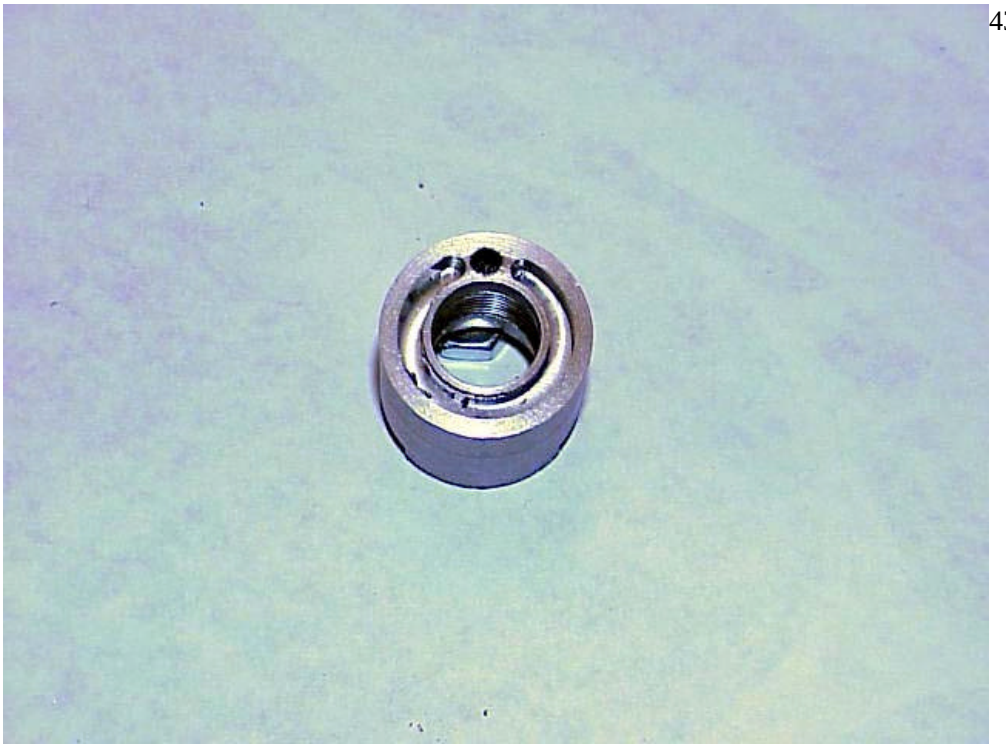

FIGURE 8a: Water-cooling Adaptor for the Low-pressure Transducer

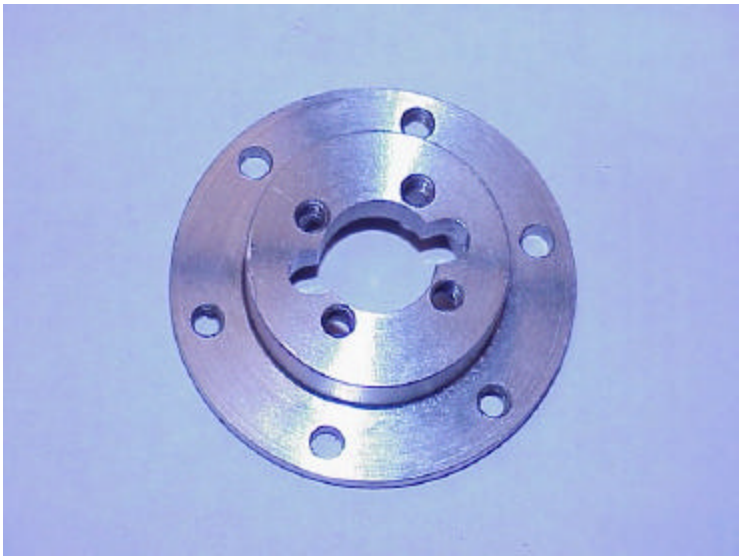

FIGURE 8b: Water-cooling Bracket to Hold Transducer Against Cylinder Wall

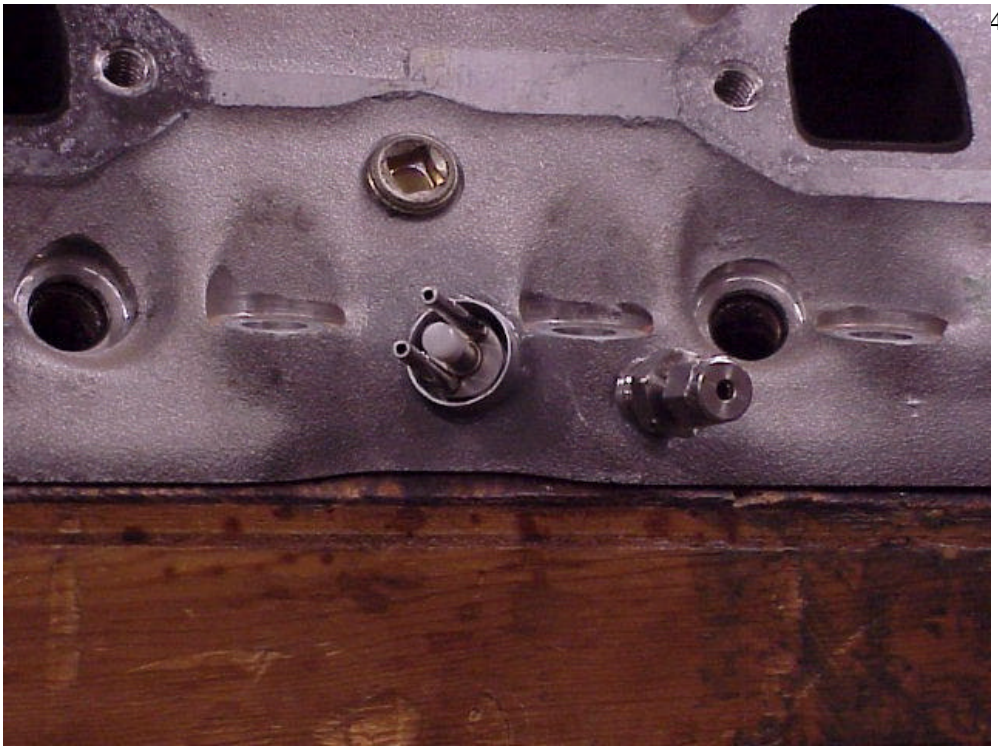

FIGURE 9: Engine Head Modification to Allow 7061 Transducer Access

FIGURE 10a: Kistler 4045 Piezo-Resistive Pressure Transducer

FIGURE 10b: Kistler 4045 Piezo-Resistive Pressure Transducer (front-view)

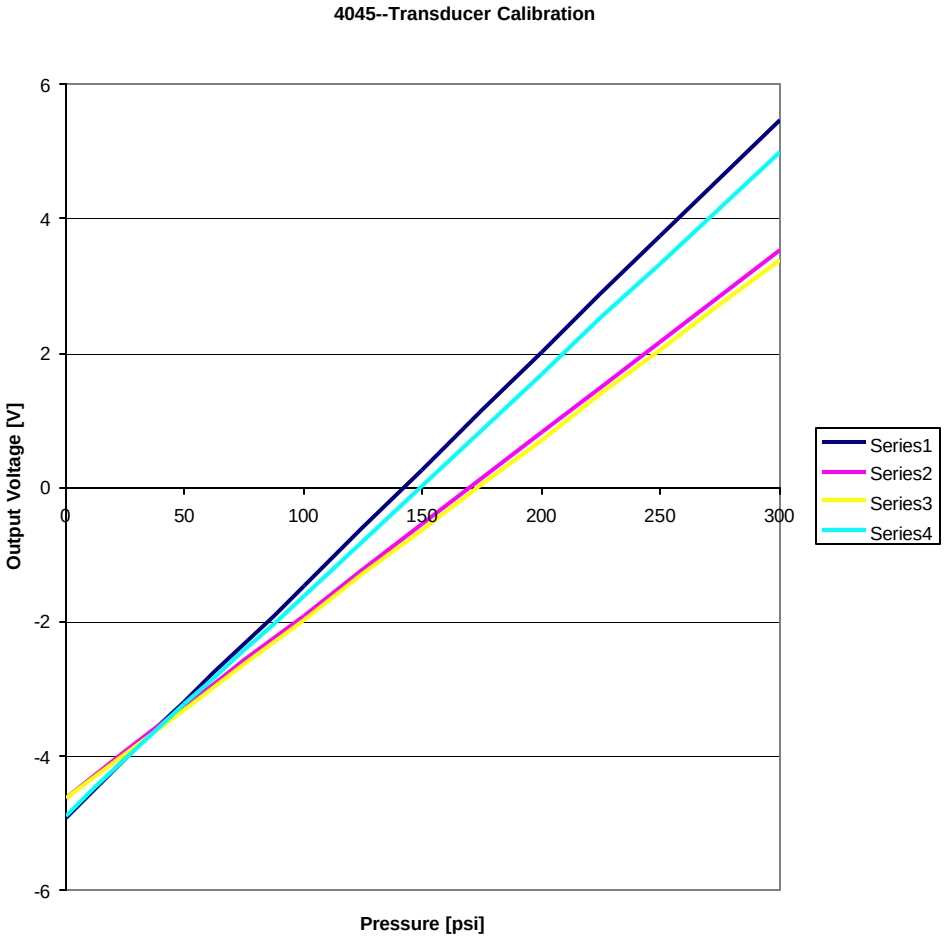

FIGURE 11: 4045 Piezo-Resistive Pressure Transducer Calibration Chart

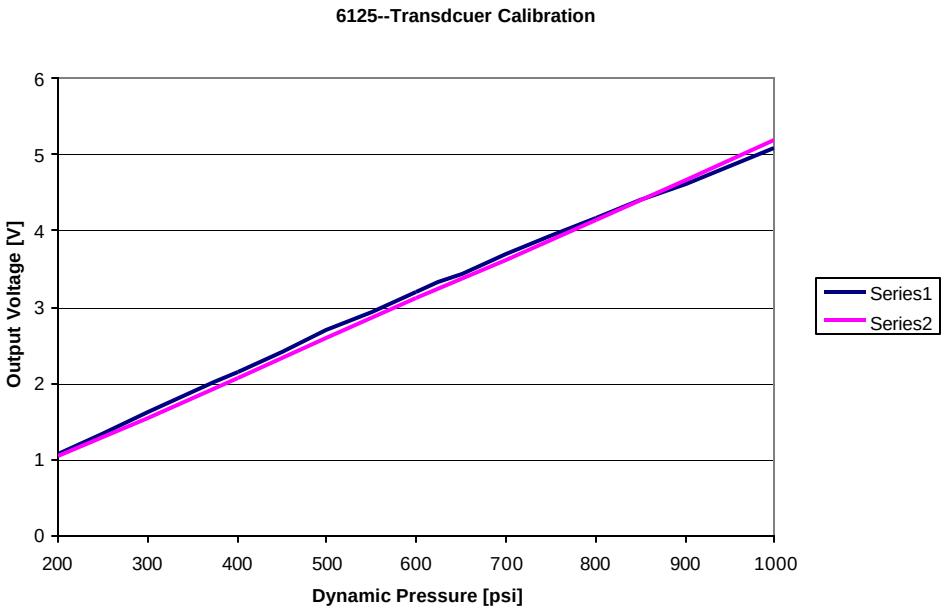

FIGURE 12: 6125 Transducer Calibration Chart

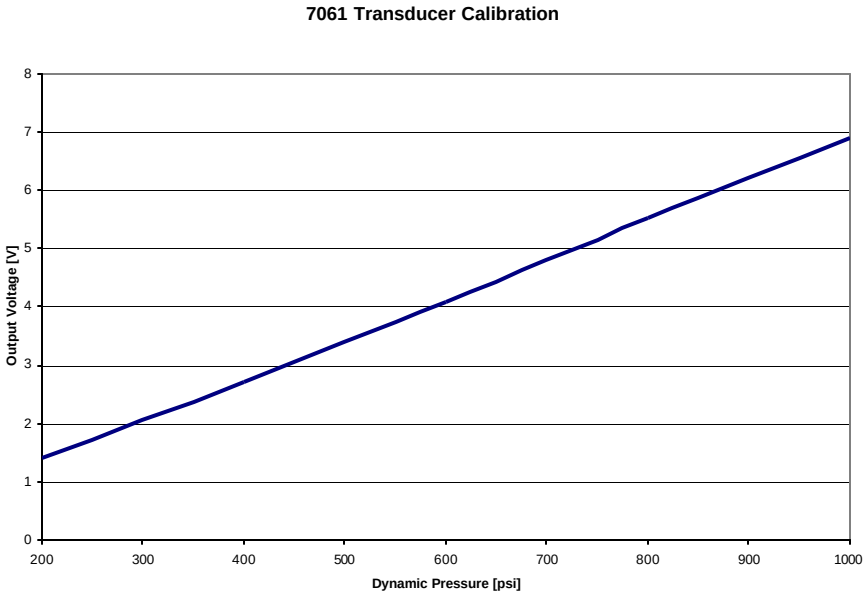

FIGURE 13: 7061 Transducer Calibration Chart

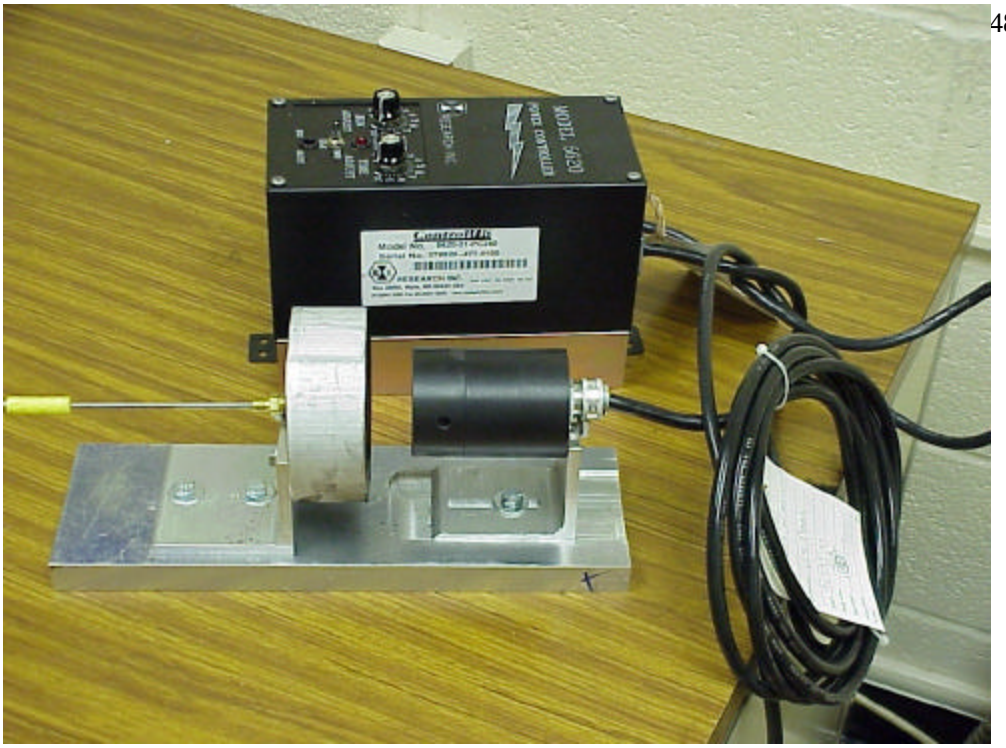

FIGURE 14a: Fast –Response Thermocouple Calibration Apparatus

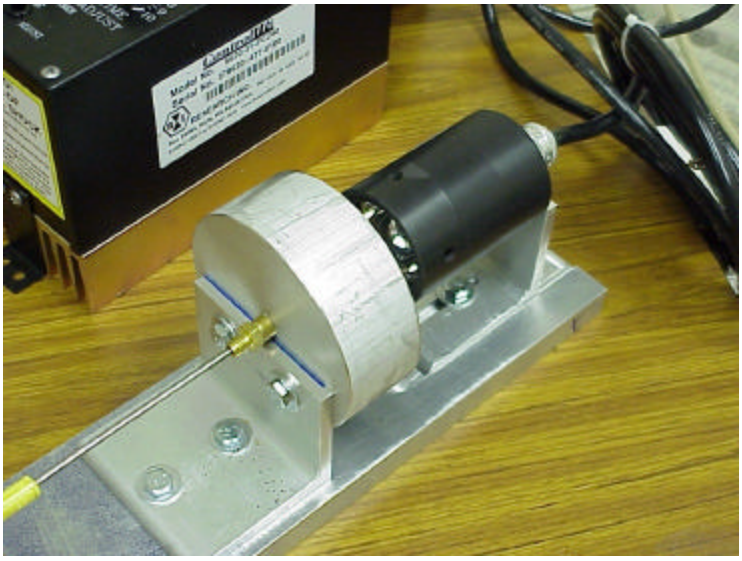

FIGURE 14b: Fast –Response Thermocouple Calibration Apparatus (side-view)

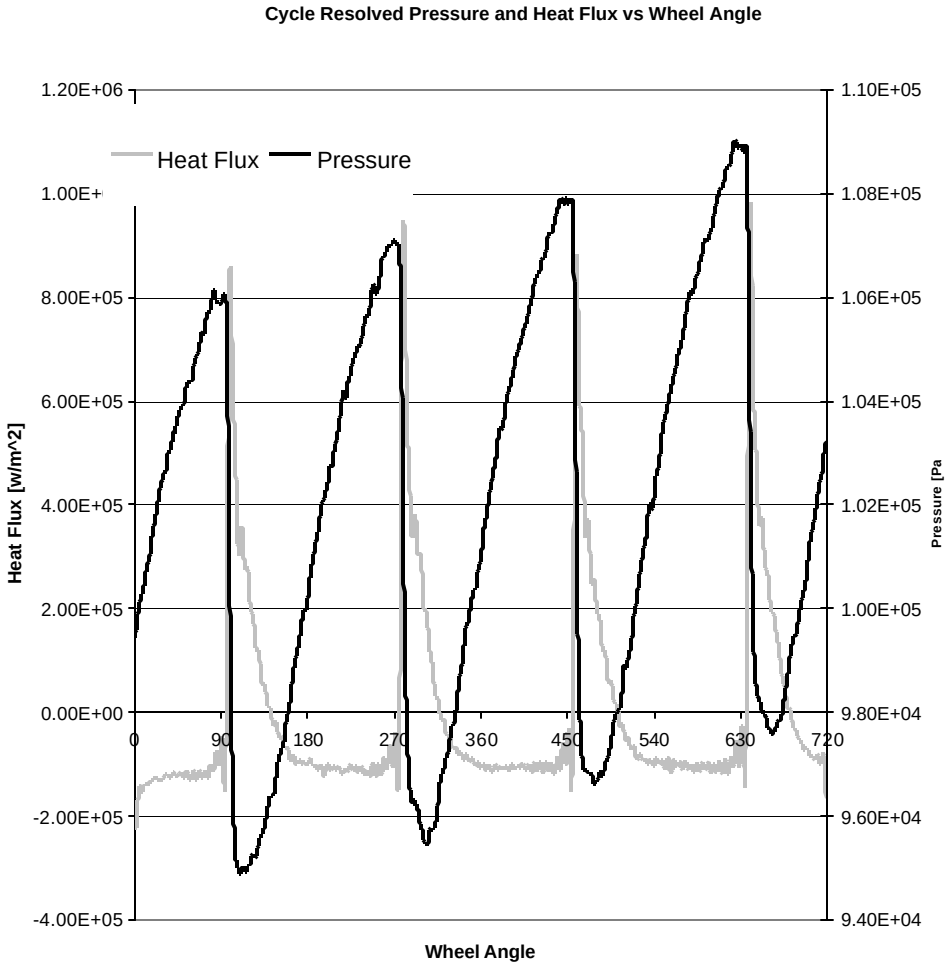

FIGURE 15: Cycle-Resolved Pressure and Heat Flux vs. Crank Angle

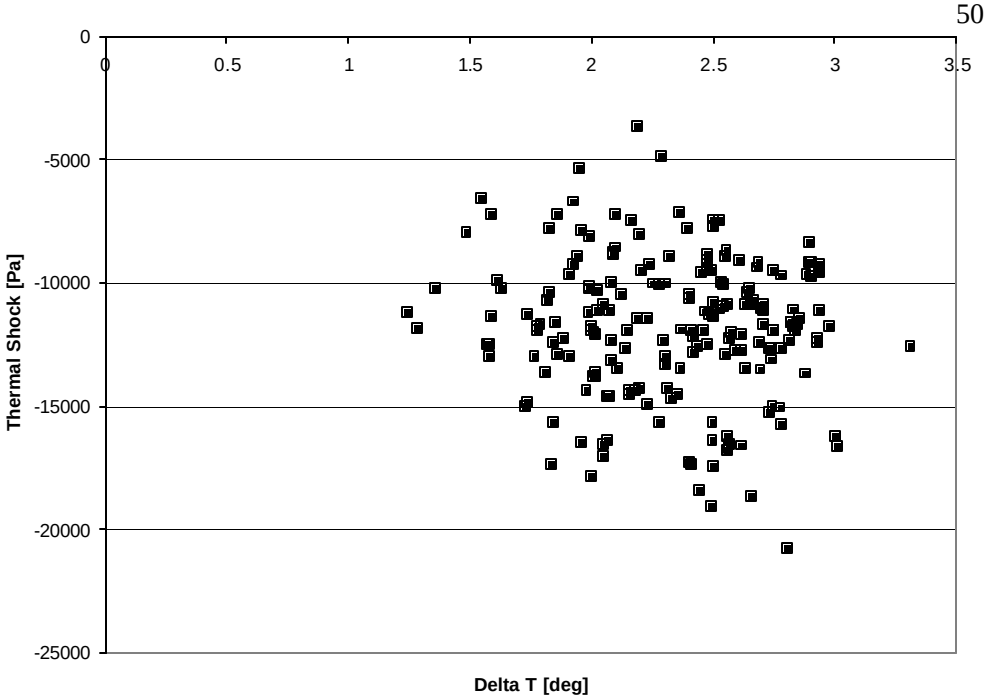

FIGURE 16: Delta Temperature vs. Thermal Shock

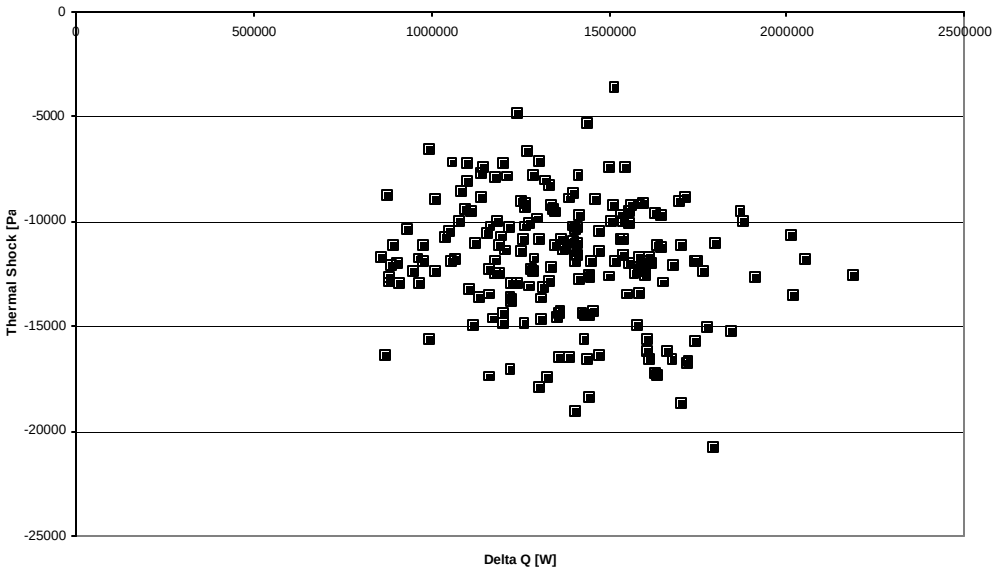

FIGURE 17: Delta Heat Flux vs. Thermal Shock

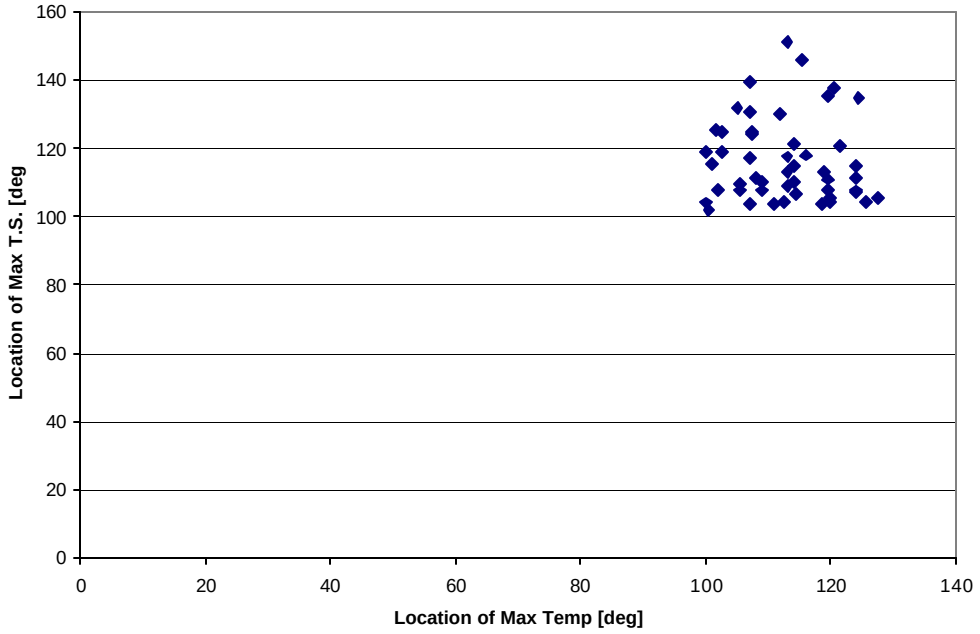

FIGURE 18: The Location of Maximum Temperature vs. the Location of Maximum Thermal Shock

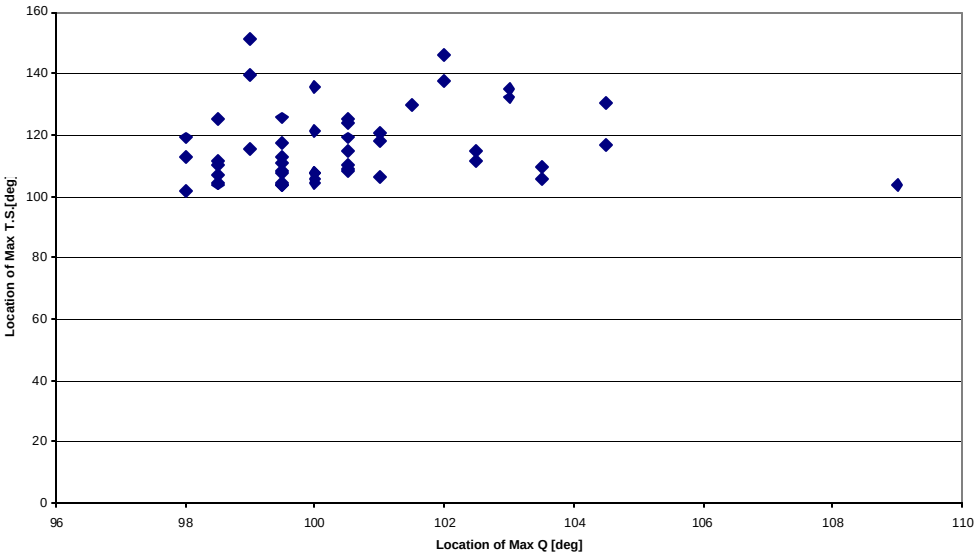

FIGURE 19: The Location of Maximum Heat Flux vs. the Location of Maximum Thermal Shock

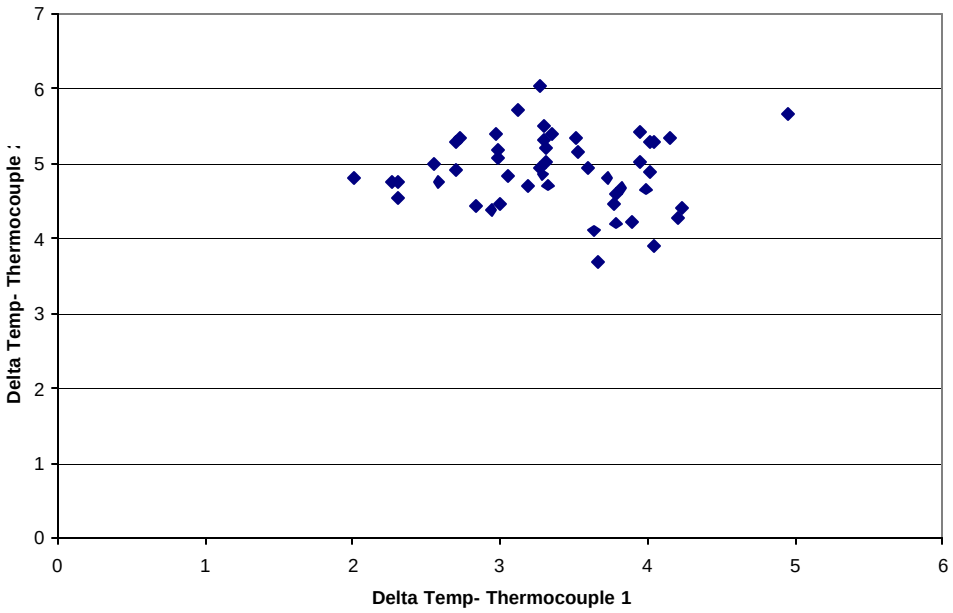

FIGURE 20: Temperature Pulse for Two Thermocouples in Housing

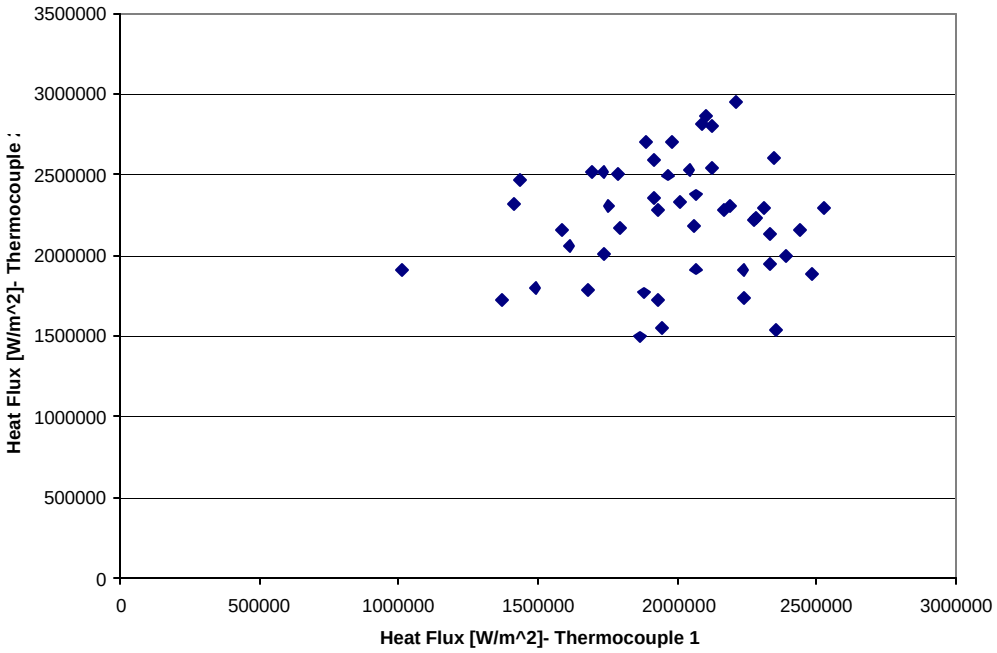

FIGURE 21: Heat Flux Pulse for Two Thermocouples in Housing

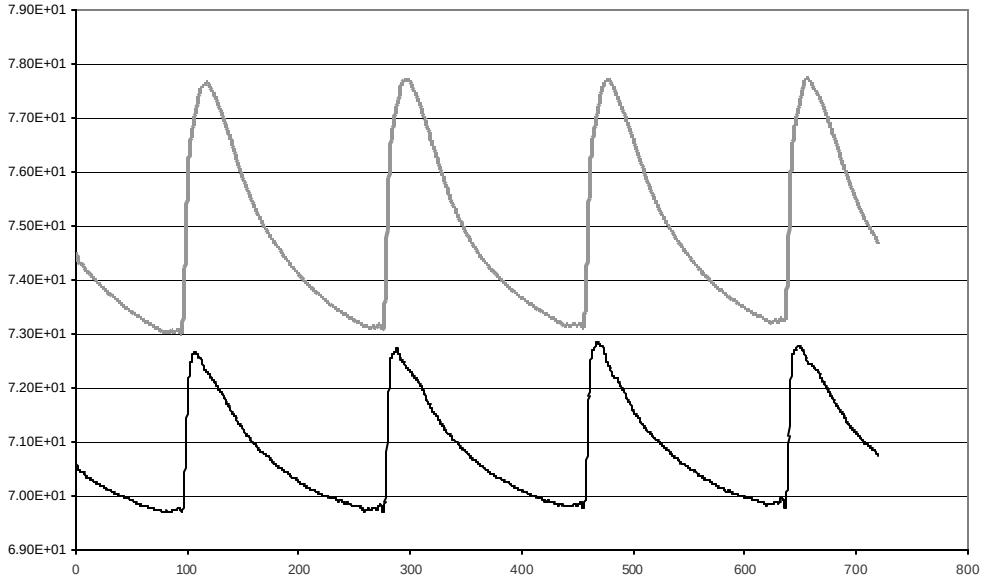

FIGURE 22: Ensemble-Averaged Cycle-Resolved Temperature History for two Thermocouples

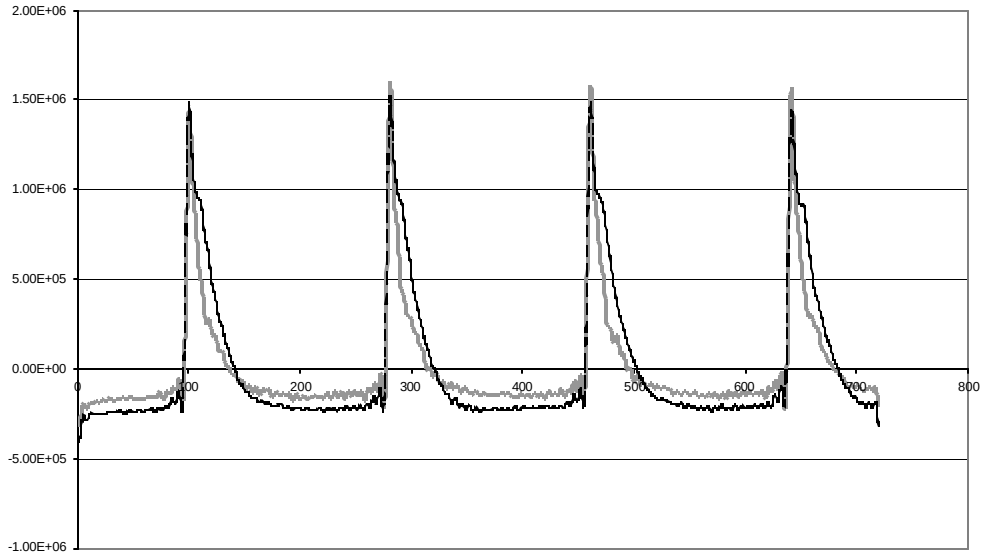

FIGURE 23: Ensemble-Averaged Cycle-Resolved Heat Flux History for two Thermocouples

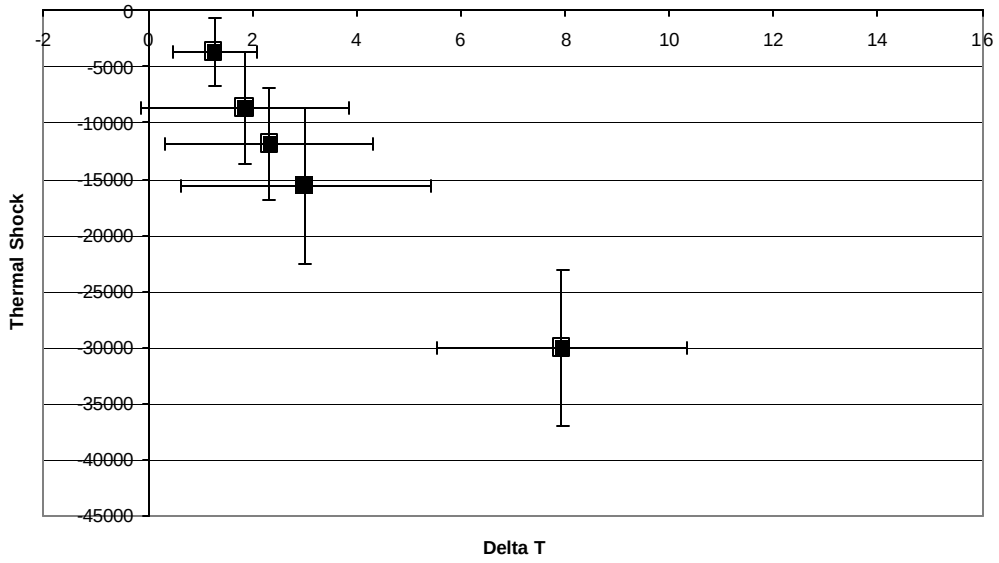

FIGURE 24: Average Temperature Pulse vs. Thermal Shock with Error Bars

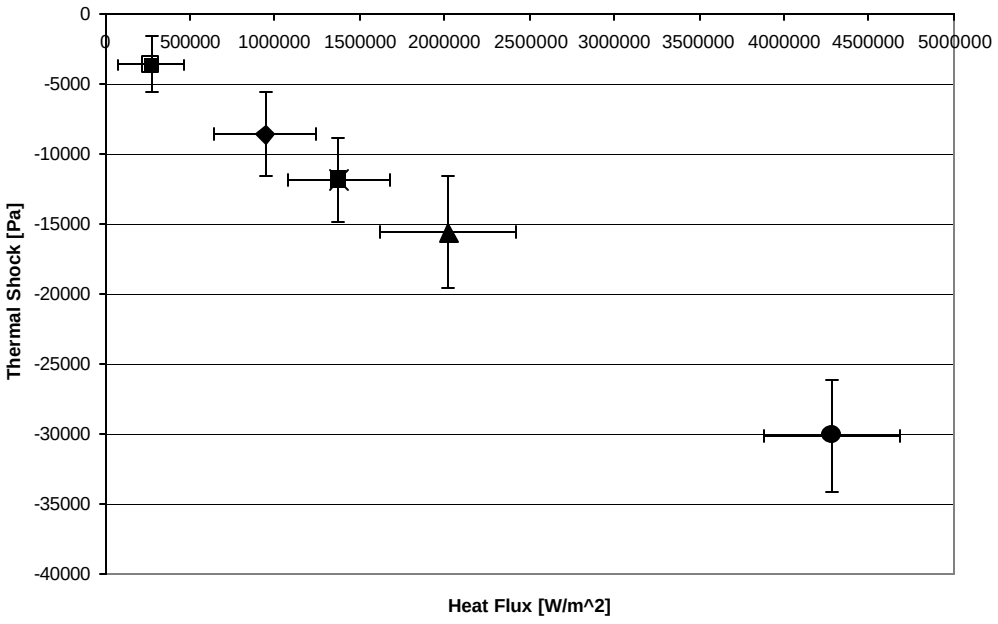

FIGURE 25: Average Heat Flux Pulse vs. Thermal Shock with Error Bars

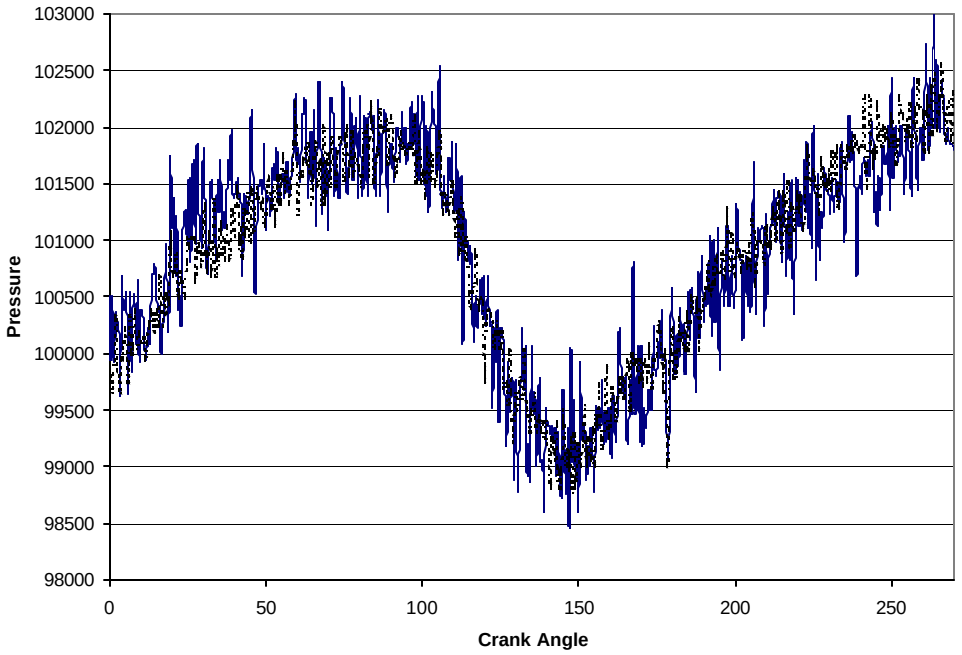

FIGURE 26: Ensemble-Conditioned Average Pressure Trace

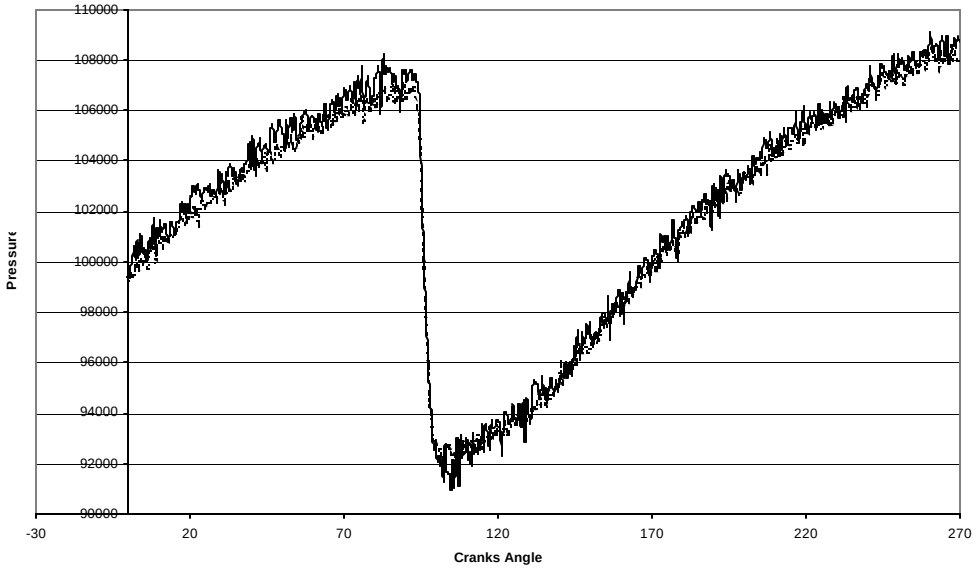

FIGURE 27: Ensemble-Conditioned Average Pressure Trace

FIGURE 28a: Comparison Photo of the 7061 and the 6125 Pressure Transducers

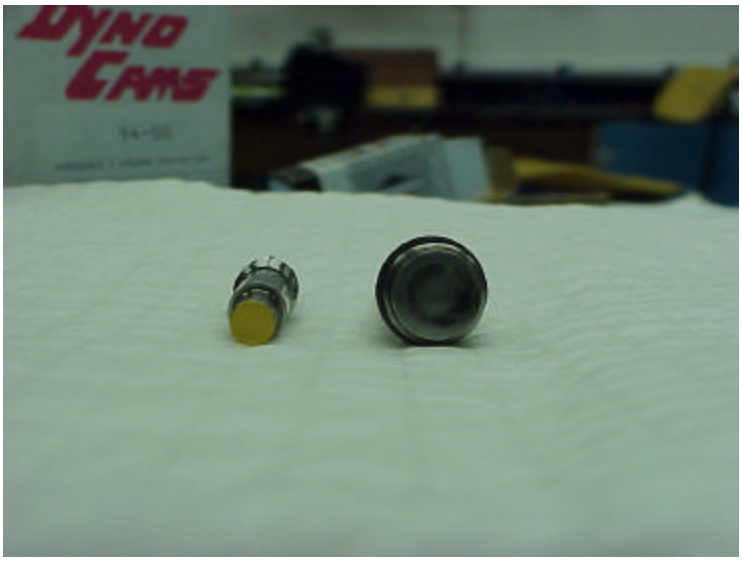

FIGURE 28b: Comparison Photo of the 7061 and the 6125 Pressure Transducers (front view)

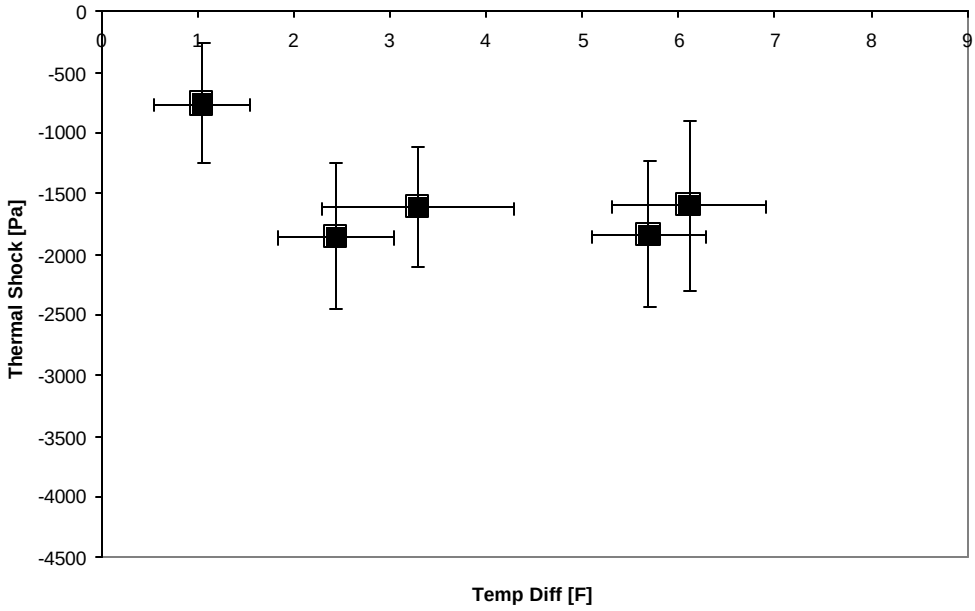

FIGURE 29a: Temperature Difference vs. Thermal Shock in 7061 Transducer

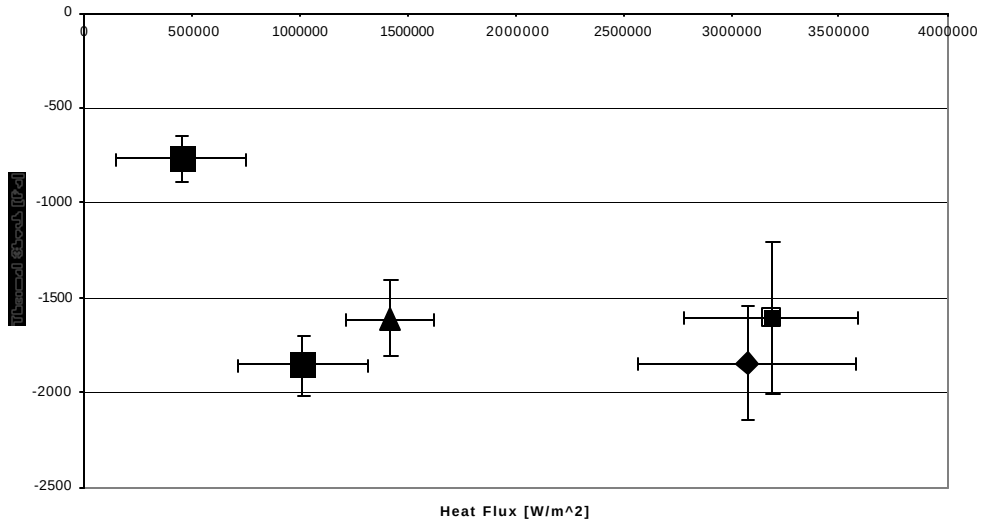

FIGURE 29b: 7061-Heat Flux vs. Thermal Shock

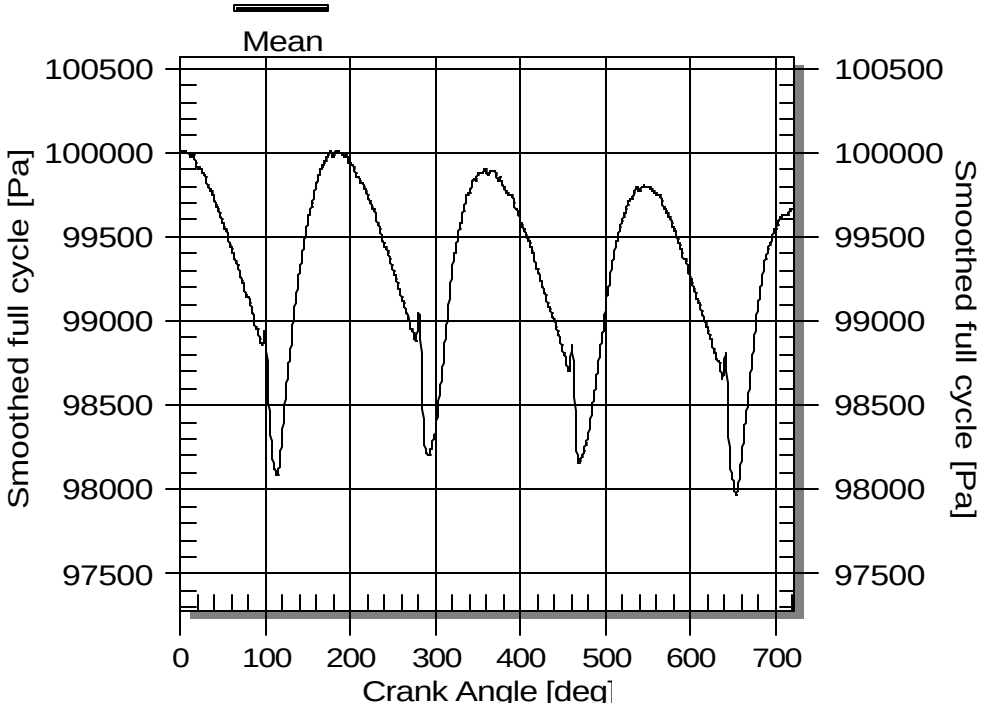

FIGURE 30: Conditioned Ensemble Average of 7061 Pressure Transducer Recovery

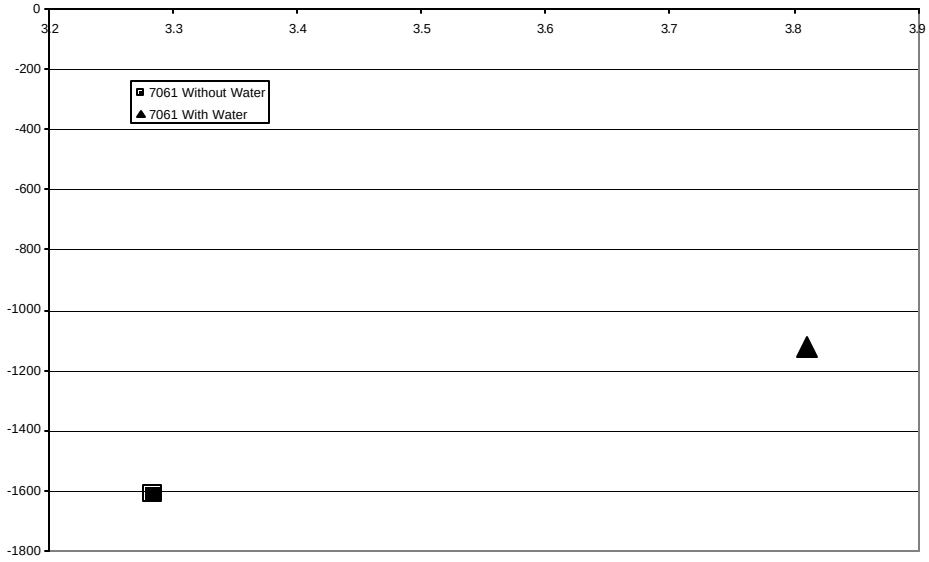

FIGURE 31: Difference of Response of the 7061 with and without Water-cooling

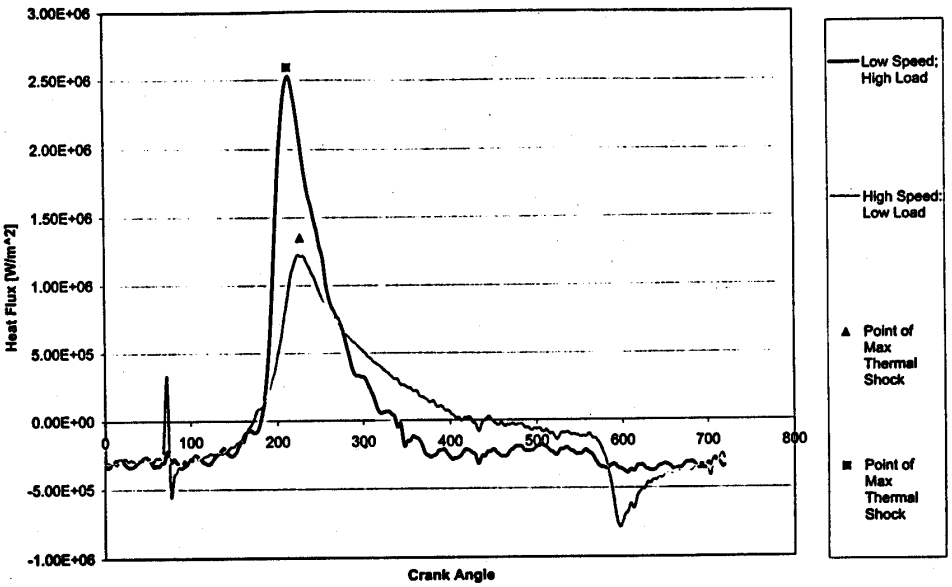

FIGURE 32: Cycle-resolved Heat Flux vs. Crank Angle for 2 Engine Conditions

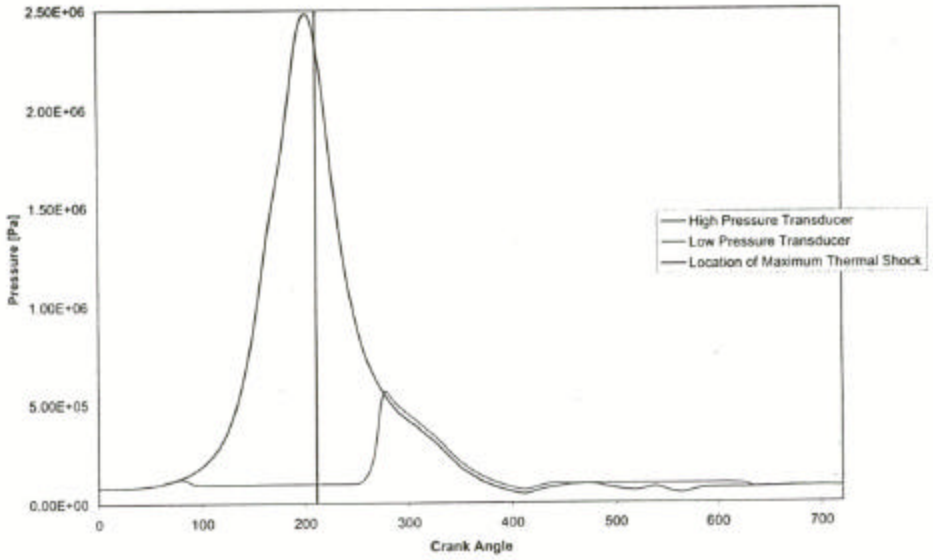

FIGURE 33: Cycle-Resolved Pressure vs. Crank Angle using Full-cycle and Reference Transducers

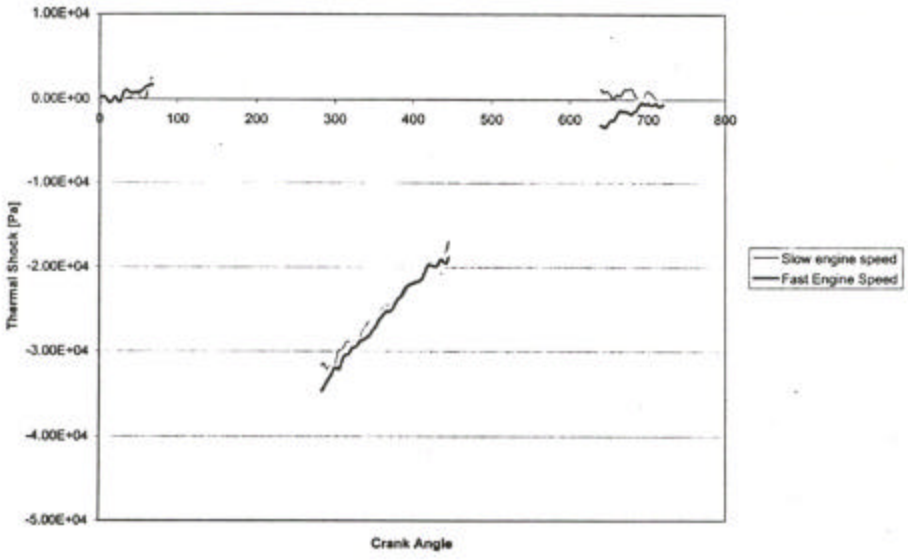

FIGURE 34: Thermal Shock for Two Engine Speeds

[1] Kuratle, R.H., Marki, B.< "Influencing Parameters and Error Sources During Indication on Internal Combustion Engines," SAE Paper#920233, 1992.

[2]Randolph, Andrew L., "Cylinder-Pressure-Transducer Mounting Techniques to Maximize Data Accuracy", SAE Paper #900171, 1990

[3] Puzinauskas, Paulius V., Eves, Joesph C. "Measuring Absolute-Cylinder Pressure and Pressure Drop Across Intake Valves of Firing Engines.", SAE PAPER #941881, 1994.

[4] Randolph, Andrew L., "Cylinder-Pressure-Transducer Mounting Techniques to Maximize Data Accuracy", SAE Paper #900171, 1990

[5] Puzinauskas, Paulius V., Eves, Joesph C. "Measuring Absolute-Cylinder Pressure and Pressure Drop Across Intake Valves of Firing Engines.", SAE PAPER #941881, 1994

[6] Randolph, Andrew L., "Cylinder-Pressure-Transducer Mounting Techniques to Maximize Data Accuracy", SAE Paper #900171, 1990

[7] Puzinauskas, Paulius v. "Combustion and Heat-Transfer Studies in a Spark-Ignition Engine." Thesis, University of Michigan, 1989.

[8] Puzinauskas, Paulius v. "Combustion and Heat-Transfer Studies in a Spark-Ignition Engine." Thesis, University of Michigan, 1989.

[9] Puzinauskas, Paulius v. "Combustion and Heat-Transfer Studies in a Spark-Ignition Engine." Thesis, University of Michigan, 1989.

[10] Randolph, A.L., "Methods of Processing Cylinder-Pressure Transducer Signals to Maximize Data Accuracy," SAE Paper #900172, 1990.